energies

MDPI

Article

Research on a Short-Circuit Current Suppression Strategy for Multi-DC Receiving-End Power Grids Integrating Fuzzy Comprehensive Evaluation and Coordinated Optimization of Grid Structure and Current-Limiting Devices

Yang Cao [1], Shanhe Liu [1], Xudong Zhang [2], Zixuan Hu [3,*], Xiaofei Li [1], Pan Gu [1], Jingyi Zhang [1] and Yan Zhang [1]

[1] State Grid Economic and Technological Research Institute Co., Ltd., No. 18 Binhe Road, Future Science Park, Changping District, Beijing 102209, China
[2] State Grid Corporation of China, No. 86 West Chang'an Avenue, Xicheng District, Beijing 100031, China
[3] School of Electrical and Electronic Engineering, North China Electric Power University, Beijing Campus, No. 2 Beinong Road, Changping District, Beijing 102206, China
* Correspondence: huzixuan10@ncepu.edu.cn

Abstract

To address excessive short-circuit currents and the pronounced "strong DC, weak AC" characteristic caused by large-scale UHVDC infeed into receiving-end grids, this paper proposes a planning-oriented suppression strategy integrating coordinated optimization of grid structure and superconducting fault current limiters (SFCLs) with fuzzy comprehensive evaluation. A coordinated model is first established to jointly determine discrete branch states and continuous SFCL equivalent series resistances while accounting for line-disconnection costs, equipment-investment costs, short-circuit-current limits, and physical-logical coupling constraints. A sensitivity-assisted Benders-type iterative framework is then developed, in which a mixed-integer master problem generates candidate planning decisions and a BPA-based subproblem performs nonlinear physical verification. Local finite-difference sensitivities are used to construct feasibility-guidance cuts rather than globally valid analytical Benders cuts. Physically feasible schemes are subsequently evaluated in terms of current-limiting effectiveness, steady-state voltage deviation, equipment-investment cost, and network loss. The method is validated using the modified CSEE-VS-66 system under standard and high-load operating conditions, a representative single-line-to-ground fault scenario, and an additional CSEE-FS-47 system. The results demonstrate that the proposed framework can provide physically feasible and economically balanced planning schemes without relying on a single performance indicator.

Keywords: multi-DC receiving-end power grid; short-circuit current suppression; coordinated optimization; superconducting fault current limiter; Benders decomposition; fuzzy comprehensive evaluation

Check for updates

Academic Editors: Pavlos S. Georgilakis and David Schoenwald

Received: 26 May 2026
Revised: 16 October 2026
Accepted: 27 October 2026
Published: 3 November 2026

Copyright: © 2026 by the authors. Licensee MDPI, Basel, Switzerland. This article is an open access article distributed under the terms and conditions of the Creative Commons Attribution (CC BY) license.

1. Introduction

As the 'dual-carbon' goals advance and new power systems are constructed, the spatial mismatch between China's energy resources and load centers has driven the rapid development of ultra-high-voltage direct-current (UHVDC) transmission technology [1]. However, the large-scale integration of multiple direct-current (DC) links into receiving-end grids creates a pronounced 'strong DC, weak alternating-current (AC)' characteristic. The resulting excessive short-circuit currents have become a bottleneck, restricting both

the safe operation of these grids and the expansion of their power-reception capacity [2,3]. During the planning of large receiving-end grids, short-circuit-current levels at certain hub substations have approached or exceeded the rated interrupting capacity of circuit breakers, posing a serious threat to system security and reliability [4,5].

Existing research and engineering practices for short-circuit-current suppression primarily focus on grid-structure adjustment and the configuration of current-limiting devices. For grid-structure optimization, opening selected lines to increase the electrical distance between stations with excessive currents is an economical option. References [6,7] redistribute short-circuit currents by adjusting branch operating-state variables and altering the sparse structure of the nodal admittance matrix. However, this approach inherently sacrifices grid connectivity. Excessive line disconnections can worsen power-flow distribution [8] and may affect the voltage- and frequency-support requirements of line-commutated-converter high-voltage direct-current (LCC-HVDC) receiving-end grids [9].

Regarding fault-current-limiting devices, solid-state and fast-switching limiter technologies are designed to insert a current-limiting impedance during a fault [10–12]. Current-limiting reactors can also affect transient protection requirements in DC networks [13]. For superconducting fault current limiter (SFCL) planning, suppression effectiveness is sensitive to installation location [14], and large-scale deployment can incur substantial equipment investment. Recent studies have therefore applied multi-objective algorithms to coordinate grid adjustments and limiter allocations, seeking a trade-off between security and economic efficiency [15,16].

Nevertheless, formulating short-circuit-current suppression strategies for large-scale receiving-end grids still faces significant challenges. First, short-circuit-current constraints are highly nonconvex and nonlinear, and the associated discrete decisions can make large planning models computationally demanding. Frequency-security issues are normally handled by dedicated controls such as adaptive under-frequency load shedding [17], which is outside the present short-circuit-current planning model. Second, existing optimization models often struggle to account simultaneously for the effects of grid changes on the overall system. Reference [18] introduced McCormick-envelope relaxations for nonlinear AC optimal-power-flow terms. Reference [19] further developed a coordinated optimization framework for limiter configuration and grid structure, achieving joint improvements in suppression effectiveness and economic cost through an iterative architecture. Compared with Reference [19], the principal change introduced by the BPA check is that a candidate plan is accepted only after its short-circuit-current feasibility has been reconfirmed using the nonlinear PSD-BPA model; the resulting local finite-difference sensitivities are then returned to the planning model as search-guidance information.

Recent studies have addressed topology adjustment and fault-current-limiter allocation as two planning routes for short-circuit-current suppression. Reference [20] developed an optimization method for limiting short-circuit current through power-grid configuration adjustment and line-opening selection; fault-current-limiter allocation was not included. Li et al. developed optimal transmission switching for multi-infeed DC receiving-end grids with explicit short-circuit-current, multi-infeed short-circuit-ratio, and single-component-outage (N-1) constraints [21], while Wu et al. formulated large-scale fault-current-limiter allocation considering transmission switching and unit commitment and solved it using heuristic decomposition [22].

This study is positioned as a planning-oriented, steady-state assessment rather than a transient-control or equipment-design study. The base optimization model evaluates root-mean-square short-circuit currents and steady-state operating quantities under specified network configurations. Accordingly, the SFCL is represented by its equivalent current-limiting series resistance after activation, whereas its triggering dynamics, recovery process,

thermal limits, and detailed coordination with protection devices are outside the model boundary. Likewise, transient AC/DC interactions, the dynamic evolution of commutation failures, post-fault voltage recovery, and frequency response are not incorporated as decision constraints in the present formulation. Consequently, the voltage-related results reported in this study refer specifically to steady-state voltage performance and should not be interpreted as evidence of transient or dynamic stability. These dynamic characteristics require dedicated electromagnetic-transient and electromechanical-dynamic studies before the proposed planning scheme is implemented in an actual power grid.

Within the above scope, this study makes two main methodological contributions. First, a planning framework is established to coordinate discrete topology adjustment and continuous SFCL equivalent-series-resistance allocation, with the short-circuit feasibility of each candidate scheme verified through nonlinear short-circuit calculations. Second, a sensitivity-guided iterative procedure is developed to transfer locally estimated short-circuit-current information from the physical-verification module to the planning model. The resulting constraints provide local search guidance rather than globally valid analytical Benders cuts. After optimization, fuzzy comprehensive evaluation is used only to compare completed short-circuit-feasible schemes and does not participate in determining the planning decisions.

2. Mathematical Model for Coordinated Optimization of Short-Circuit Current Suppression in Multi-DC Receiving-End Grids

2.1. Decision Variables

Constructing a mathematical model for short-circuit current suppression in a multi-DC receiving-end power grid requires defining decision variables that accurately characterize grid topology and current-limiting configurations. Fundamentally, short-circuit current suppression enlarges the equivalent electrical distance of fault paths by altering the network admittance distribution.

To characterize planning-stage reconfiguration of the grid structure, a binary integer variable x_l is introduced to represent the operating status of each branch l in the candidate-branch set Ω_L. When $x_l = 1$, the branch l remains closed in operation; when $x_l = 0$, the branch is opened to block the high-admittance path of fault current.

To represent the resistive component inserted by an SFCL after activation, the continuous variable R_l denotes the per-unit (p.u.) equivalent series resistance assigned to candidate branch $l \in \Omega_L$. A binary installation variable z_l is introduced to distinguish a closed branch without an SFCL from a closed branch equipped with one:

$$z_l \in \{0, 1\}, \qquad \forall l \in \Omega_L, \tag{1}$$

In this study, R_l is the equivalent series resistance inserted after the SFCL enters its current-limiting state; it is not the total complex branch impedance. The binary variable $z_l = 1$ denotes an installed SFCL, whereas $z_l = 0$ denotes that no SFCL is installed. The planning model evaluates root-mean-square (RMS) short-circuit current under a specified network configuration. Triggering dynamics, recovery, and thermal response remain outside the present scope and require electromagnetic-transient verification during equipment design.

The variables x_l, z_l, and R_l jointly represent the branch operating state, the SFCL installation decision, and the inserted equivalent series resistance, respectively.

Considering both grid adjustment and the installation of current-limiting devices, the equivalent admittance y_l^{eq} of branch l must be expressed carefully to avoid a numerical

singularity when the branch is opened. A virtual minimum conductance parameter G_{open} is therefore introduced:

$$y_l^{eq} = x_l \cdot (y_l^{-1} + R_l)^{-1} + (1 - x_l) \cdot G_{open}, \tag{2}$$

where y_l is the original complex series admittance of branch l, y_l^{-1} is its series impedance, R_l is the inserted real series resistance in per unit, and $G_{\text{open}} = 10^{-5}$ p.u. is the virtual conductance assigned to an open branch. Thus, $y_l^{\text{eq}} = (y_l^{-1} + R_l)^{-1}$ for $x_l = 1$ and $y_l^{\text{eq}} = G_{\text{open}}$ for $x_l = 0$. The small nonzero conductance regularizes repeated topology updates but does not constitute a mathematical guarantee of solver convergence or global optimality.

Finally, the model introduces a nonnegative short-circuit-current violation slack s_i for monitored bus i. It measures the temporary excess of the calculated current $I_{\text{sc},i}$ over the interrupting-capacity limit $I_{\text{limit},i}$ and satisfies:

$$I_{\text{sc},i}(x, R) - s_i \le I_{\text{limit},i}, \qquad s_i \ge 0, \quad \forall i \in \Omega_B, \tag{3}$$

This slack variable allows temporary limit violations during early optimization stages. Guided by the penalty term in the objective function, the slack variable provides violation information that can be used to construct local sensitivity-guidance constraints and direct the iterative process toward a solution satisfying the prescribed short-circuit-current limits. Its introduction serves as a feasibility-restoration mechanism during the iterative solution process and does not by itself establish global convergence or global optimality.

2.2. Objective Function

Short-circuit current suppression requires balancing system reliability, equipment investment, and security, rather than merely satisfying physical constraints. This section constructs a coordinated optimization model to minimize the comprehensive socioeconomic cost. The objective function comprises grid-reconfiguration costs, SFCL investment costs, and a penalty term to ensure feasibility:

$$\min F = \sum_{l \in \Omega_L} C_l^{\text{line}}(1 - x_l) + \sum_{l \in \Omega_L} C_l^{\text{SFCL}} R_l + \rho s, \tag{4}$$

where Ω_L is the candidate-branch set; C_l^{line} is the equivalent planning-cost coefficient associated with opening branch l; C_l^{SFCL} is the SFCL investment-cost coefficient per unit equivalent series resistance; ρ is the violation-penalty coefficient; and $s = \sum_{i \in \Omega_B} s_i$ is the aggregate nonnegative short-circuit-current violation. The penalty coefficient must be scaled relative to the investment terms to avoid numerical swamping.

In the proposed model, ρ is set as $\rho = 10^3 \max_{l \in \Omega_L}\{C_l^{\text{line}}, C_l^{\text{SFCL}} R_{\max}\}$, where $R_{\max}$ is the upper bound on the installed SFCL equivalent series resistance. This scaling gives current-limit violations a substantially higher penalty than ordinary investment variations and encourages feasibility restoration before further cost reduction. It does not, by itself, guarantee convergence or global optimality.

The construction logic and physical meaning of the objective function are detailed as follows:

1. Robustness cost of grid reconfiguration: A strongly interconnected structure supports the steady-state voltage profile and reactive-power transfer capability of the receiving-end grid. Penalizing branch disconnection therefore discourages excessive topology adjustment while preserving the option to open electrically influential corridors. This planning-cost term is an economic surrogate for the consequences of structural change; it does not replace the physical short-circuit verification or the post-planning operating checks defined below.

2. Marginal investment cost of current-limiting equipment: SFCL investment is represented as a linear function of the per-unit equivalent series resistance R_l. The term combines the equivalent costs of superconducting materials, refrigeration capacity, and installation and creates a transparent trade-off with the grid-reconfiguration term. For a severe current violation, the model compares the marginal current-reduction benefit of topology adjustment and SFCL investment while guiding the plan back toward the prescribed current-feasible region.
3. Softening of security constraints and convergence guidance: The slack variable and penalty term are crucial for solving the large-scale mixed-integer nonlinear programming (MINLP) problem. The short-circuit-current constraint boundary is highly nonlinear because the topology variables and SFCL series-resistance variables jointly modify the nodal admittance matrix and the resulting fault-current distribution. Imposing hard constraints early in the iterative process may result in an empty feasible region. The $\rho \cdot s$ term permits temporary current-limit violations during the search. The violation information obtained from the physical-verification subproblem is subsequently used to construct local sensitivity-guidance constraints for the master problem. These constraints guide the subsequent iterations toward the short-circuit-feasible region; however, the penalty term and the locally constructed guidance constraints do not by themselves establish global convergence or global optimality for the original nonconvex problem.

2.3. Constraints

The coordinated optimization model must satisfy power system physical laws, ensure logical consistency between topology changes and SFCL configurations, and maintain secure operating boundaries. The primary constraints are detailed below:

1. Short-circuit current security constraints
   Suppressing excessive short-circuit currents at key buses is the model's core objective. For the monitored-bus set Ω_B, the RMS three-phase short-circuit current must satisfy:

$$I_{\mathrm{sc},i}(x, R) \le I_{\mathrm{limit},i} + s_i, \qquad \forall i \in \Omega_B, \tag{5}$$

   where $x = [x_l]_{l\in\Omega_L}$ and $R = [R_l]_{l\in\Omega_L}$ are the branch-status and SFCL-resistance vectors, respectively; $I_{\mathrm{sc},i}(x, R)$ is the calculated RMS short-circuit current at bus i; $I_{\mathrm{limit},i}$ is its interrupting-capacity limit; and s_i is the nonnegative slack defined above. Because $I_{\mathrm{sc},i}$ depends nonlinearly on x and R through the bus-impedance matrix Z_{bus}, the following local first-order approximation is used to guide the iterative search:

$$I_i^{(k)} + \sum_{l\in\Omega_L} G_{i,l}^{(k)}(x_l - x_l^{(k)}) + \sum_{l\in\Omega_L} H_{i,l}^{(k)}(R_l - R_l^{(k)}) \le I_{\mathrm{limit},i} + s_i, \tag{6}$$

   where k is the iteration index; $I_i^{(k)} = I_{\mathrm{sc},i}(x^{(k)}, R^{(k)})$ is the current evaluated at the iteration point $(x^{(k)}, R^{(k)})$; $G_{i,l}^{(k)}$ is the local finite state-change coefficient associated with toggling branch-status variable x_l; and $H_{i,l}^{(k)}$ is the local finite-difference coefficient associated with R_l. These coefficients describe only the response near the evaluated point and are not global derivatives of the nonconvex model.
   The principal formulation uses the RMS three-phase short-circuit current. To avoid implying that one common plan is optimized simultaneously for different fault types, the three-phase and single-line-to-ground (SLG) faults are defined as independent planning cases that share the same candidate set, cost coefficients, and current limit.

$$\Omega_F^{\mathrm{case}} = \{f\}, \qquad f \in \{f_{3\phi}, f_{\mathrm{SLG}}\}, \tag{7}$$

$$\left(x^{(f)}, R^{(f)}\right) = \arg\min_{x,R}\left[C_{\mathrm{open}}(x) + C_{\mathrm{SFCL}}(R)\right], \tag{8}$$

where $f^{3\phi}$ and f^{SLG} denote the three-phase and SLG fault cases, respectively; Ω_F^{case} is the singleton fault set solved in one run; $(x^{(f)}, R^{(f)})$ is the plan obtained for fault case f; C_{open} and C_{SFCL} are the topology-adjustment and SFCL-investment components of the objective; and $I_{i,f}(x^{(f)}, R^{(f)})$ is the RMS current at bus i under fault case f. For the plan obtained independently for fault case f, the corresponding short-circuit currents must satisfy:

$$I_{i,f}\left(x^{(f)}, R^{(f)}\right) \le I_{\mathrm{limit},i}, \quad \forall i \in \Omega_B, \quad f \in \{f^{3\phi}, f^{\mathrm{SLG}}\}, \tag{9}$$

Equation (9) is applied separately to each singleton fault set $\Omega_F^{\mathrm{case}} = \{f\}$; therefore, the three-phase and SLG cases are not required to share one common planning solution.

2. Logical coupling constraints between grid topology and current-limiting devices

To ensure physical consistency, an SFCL can be installed only on an in-service branch, and an installed SFCL must have an equivalent series resistance within the specified nonzero interval. The master problem therefore includes the following constraints:

$$z_l \le x_l, \qquad R_{\min} z_l \le R_l \le R_{\max} z_l, \qquad z_l \in \{0,1\}, \quad \forall l \in \Omega_L, \tag{10}$$

If $x_l = 0$, the constraint $z_l \le x_l$ forces $z_l = 0$ and hence $R_l = 0$. If $x_l = 1$ and $z_l = 0$, the branch remains closed without an SFCL. If $x_l = 1$ and $z_l = 1$, the installed equivalent series resistance satisfies $R_{\min} \le R_l \le R_{\max}$. This formulation explicitly retains the zero/no-device option and the minimum nonzero resistance in the master problem.

3. Normal-state operating conditions and selected-outage screening

Grid adjustments must account for supply reliability and equipment limits. Within the optimization model, the number of opened branches is explicitly limited as follows:

$$\sum_{l \in \Omega_L} (1 - x_l) \le N_{\mathrm{open,max}}, \tag{11}$$

where $N_{\mathrm{open,max}}$ is the prescribed maximum number of candidate branches that may be opened. The separate bounds $R_{\min}$ and $R_{\max}$ in Equation (10) define the minimum nonzero and maximum permissible equivalent series resistances of an installed SFCL, respectively.

Together, the logical constraints preserve the no-device state $R_l = 0$, prevent an installed SFCL from taking an arbitrarily small positive resistance, and exclude installation on an opened branch.

The opening-count limit cannot by itself characterize the consequences of topology adjustment. Each completed plan is therefore subjected to nonlinear short-circuit verification, and the coordinated scheme is additionally examined through post-optimization screening of selected single-component outages. The screening checks whether the prescribed current limit is satisfied for the specified line, generator, and HVDC-link outages.

For a data-complete normal-state assessment c_0, the active- and reactive-power balance equations are:

$$\begin{cases} P^G_{i,c_0} + P^{\mathrm{DC}}_{i,c_0} - P^D_{i,c_0} = \sum_{j \in \mathcal{N}_i} P_{ij,c_0} \\ Q^G_{i,c_0} + Q^{\mathrm{DC}}_{i,c_0} - Q^D_{i,c_0} = \sum_{j \in \mathcal{N}_i} Q_{ij,c_0} \end{cases}, \qquad \forall i \in \Omega_B, \tag{12}$$

where c_0 denotes the intact normal operating state; P^G_{i,c_0} and Q^G_{i,c_0} are generator injections at bus i; P^{DC}_{i,c_0} and Q^{DC}_{i,c_0} are signed HVDC injections; P^D_{i,c_0} and Q^D_{i,c_0} are bus demands;

P_{ij,c_0} and Q_{ij,c_0} are the active- and reactive-power flows from bus i to adjacent bus j; and $\mathcal{N}_i$ is the set of buses connected to bus i.

$$\begin{cases} U_i^{\min} \le U_{i,c_0} \le U_i^{\max}, & \forall i \in \Omega_B \\ |S_{ij,c_0}| \le S_{ij}^{\max}, & \forall (i,j) \in \Omega_L \\ P_g^{\min} \le P_{g,c_0}^G \le P_g^{\max}, & \forall g \in \Omega_G \\ Q_g^{\min} \le Q_{g,c_0}^G \le Q_g^{\max}, & \forall g \in \Omega_G \\ P_{i,c_0}^{\text{shed}} = 0, & \forall i \in \Omega_B \end{cases}, \tag{13}$$

where U_{i,c_0} is the voltage magnitude at bus i with limits $U_i^{\min}$ and $U_i^{\max}$; S_{ij,c_0} is the apparent branch flow with rating $S_{ij}^{\max}$; P_{g,c_0}^G and Q_{g,c_0}^G are the active- and reactive-power outputs of generator $g \in \Omega_G$ with the stated capability limits; and P_{i,c_0}^{shed} is load shedding. These equations define the desired normal-state assessment conditions.

Let Ω_C^{line}, Ω_C^{gen}, and Ω_C^{HVDC} denote the preselected in-service single-line, single-generator, and single-HVDC-link outage sets, respectively. Their union is:

$$\Omega_C = \Omega_C^{\text{line}} \cup \Omega_C^{\text{gen}} \cup \Omega_C^{\text{HVDC}}, \tag{14}$$

Only one in-service component is removed in each screening case $c \in \Omega_C$. The corresponding component-state conditions are

$$\begin{cases} x_{l,c} = 0, & c = c_l \in \Omega_C^{\text{line}} \\ P_{g,c}^G = Q_{g,c}^G = 0, & c = c_g \in \Omega_C^{\text{gen}} \\ P_{d,c}^{\text{DC}} = Q_{d,c}^{\text{DC}} = 0, & c = c_d \in \Omega_C^{\text{HVDC}} \end{cases}, \tag{15}$$

where c_l, c_g, and c_d identify the outage of line l, generator g, and HVDC link d, respectively, while all non-outaged components retain their case-specific states. For each selected outage, $I_{\text{sc},i,c}(x,R)$ denotes the recalculated short-circuit current at monitored bus i in case c, and the screening metric is:

$$I_{\max,c} = \max_{i \in \Omega_B} I_{\text{sc},i,c}(x,R), \qquad c \in \Omega_C, \tag{16}$$

A selected outage passes the short-circuit-current screening when

$$I_{\max,c} \le I_{\text{limit}}, \qquad \forall c \in \Omega_C, \tag{17}$$

Passing the stated condition means that no selected outage exceeds the 63.0 kA short-circuit-current limit. The result is reported only for the selected contingency set and the current criterion. Planned-line reclosure, SFCL non-insertion, contingency-state voltage, branch loading, generator capability, and load service are outside the present screening scope.

Detailed relay-setting and protection-coordination constraints are not included in the present planning model. These settings require separate recalculation and coordination during the equipment-design and engineering-implementation stages.

4. Local sensitivity-guidance constraints

Because the linear master model does not represent the nonlinear physical response exactly, a local sensitivity-guidance constraint is added after a candidate violates the current limit. The constraint is constructed around the evaluated point and is used only to redirect the next master-problem solution.

$$\alpha \ge \text{Viol}^{(k)} + \sum_{l \in \Omega_L} \frac{\partial \text{Viol}}{\partial x_l}(x_l - x_l^{(k)}) + \sum_{l \in \Omega_L} \frac{\partial \text{Viol}}{\partial R_l}(R_l - R_l^{(k)}), \tag{18}$$

where $\mathrm{Viol}(x,R) = \max_{i\in\Omega_B}\{0, I_{\mathrm{sc},i}(x,R) - I_{\mathrm{limit},i}\}$ is the maximum nonnegative current violation, $\mathrm{Viol}^{(k)} = \mathrm{Viol}(x^{(k)}, R^{(k)})$, and α is an auxiliary variable carrying the locally approximated violation. The partial-derivative symbols denote finite-change estimates evaluated at iteration k. The constraint excludes or redirects nearby infeasible candidates but does not prove monotonic improvement, global convergence, or global optimality.

3. Coordinated Solution Algorithm Based on a Sensitivity-Assisted Benders-Type Procedure

3.1. Master-Subproblem Decomposition Architecture

The strong nonlinear coupling between discrete grid-topology decisions and physical short-circuit-current constraints transforms the coordinated optimization model into a large-scale mixed-integer nonlinear programming (MINLP) problem. This section therefore introduces a sensitivity-assisted Benders-type procedure that separates a linear master problem (MP), which selects the planning variables, from a nonlinear physical-verification subproblem (SP), which evaluates short-circuit feasibility.

The information exchanged between the two modules is defined explicitly. At iteration k, the MP sends the candidate topology $x^{(k)}$ and SFCL equivalent-series-resistance vector $R^{(k)}$ to the nonlinear short-circuit-calculation SP. The SP returns the recalculated current vector $I_{\mathrm{sc}}^{(k)}$ and maximum violation $\Phi^{(k)}$. If the current criterion is not satisfied, the locally estimated coefficients $S^{x,k}$ and $S^{R,k}$ are used to construct the next sensitivity-guidance constraint. Figure 1 shows the forward candidate transfer and local feedback.

The MP searches the linearized mixed discrete-continuous planning region. Formulated as a mixed-integer linear programming (MILP) model, it comprises the investment objective, topology and SFCL logical constraints, and local sensitivity-guidance constraints returned by the SP:

$$\begin{cases} \min \quad F_{\mathrm{MP}} = \sum\limits_{l\in\Omega_L} C_l^{\mathrm{line}}(1-x_l) + \sum\limits_{l\in\Omega_L} C_l^{\mathrm{SFCL}} R_l + \alpha \\ \quad \text{s.t.} \quad \sum\limits_{l\in\Omega_L}(1-x_l) \le N_{\mathrm{open,max}}, \\ \qquad z_l \le x_l, \qquad R_{\min} z_l \le R_l \le R_{\max} z_l, \qquad z_l \in \{0,1\}, \\ \qquad \alpha \ge \Phi^{(m)} + \sum\limits_{l\in\Omega_L} \dfrac{\partial \Phi^{(m)}}{\partial x_l}\left(x_l - x_l^{(m)}\right) + \sum\limits_{l\in\Omega_L} \dfrac{\partial \Phi^{(m)}}{\partial R_l}\left(R_l - R_l^{(m)}\right), \\ \qquad m = 1, 2, \ldots, k-1. \end{cases} \tag{19}$$

where F_{MP} is the MP objective; $N_{\mathrm{open,max}}$ is the opening-count limit; z_l, x_l, and R_l are the installation, branch-status, and SFCL-resistance variables; α is the auxiliary violation variable; m indexes previously evaluated candidates; and $\Phi^{(m)}$ and its finite-change coefficients provide local SP feedback.

Through the logical coupling constraints, the MP maintains consistency between SFCL allocation and the operating status of the corresponding branch. By accumulating local sensitivity-guidance constraints, the MP progressively adjusts its candidate decisions according to the violation information returned by the SP. These constraints provide an iterative approximation of the short-circuit-feasibility boundary around the previously evaluated operating points; they are not interpreted as globally valid analytical Benders cuts for the original nonconvex problem.

Correspondingly, the SP evaluates the physical short-circuit response of the trial plan $(x^{(k)}, R^{(k)})$ supplied by the MP. It does not introduce a second set of planning decisions; instead, it calculates the aggregate violation metric:

$$\Phi^{(k)} = \sum_{i \in \Omega_B} \Delta I_i^{(k)}, \qquad \Delta I_i^{(k)} = \max\{0,\, I_{\mathrm{sc},i}(x^{(k)}, R^{(k)}) - I_{\mathrm{limit},i}\}, \tag{20}$$

where $\Delta I_i^{(k)}$ is the nonnegative current violation at monitored bus i and $\Phi^{(k)}$ is the aggregate violation returned to the MP. Local first-order coefficients with respect to x_l and R_l are then estimated by finite changes in the physical model. They are numerical guidance coefficients rather than exact dual variables.

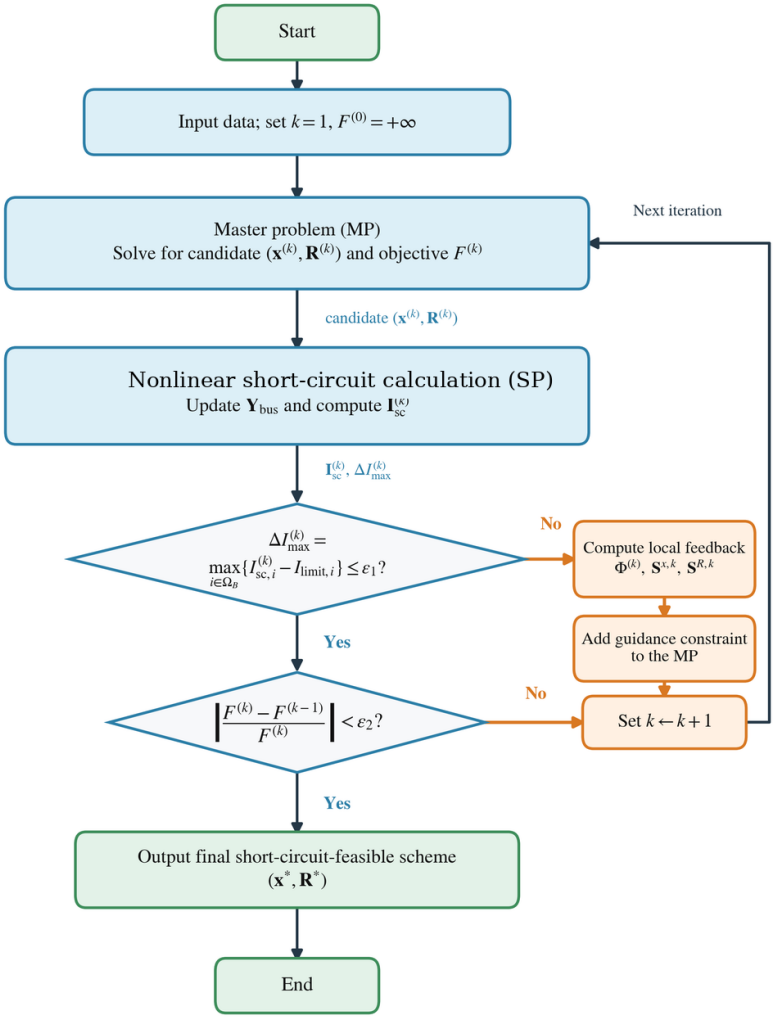


Figure 1. Information exchange between the MP and the nonlinear short-circuit-calculation SP in the sensitivity-assisted Benders-type procedure.

3.2. Generation of Cuts Based on Differential Sensitivity

Fundamentally, short-circuit-current suppression increases the equivalent transfer impedance from the fault location to the source side. During the sensitivity-assisted Benders-type iterations, the SP identifies physical violations through simulation-based verification. Sensitivity analysis then provides a local first-order approximation of the nonlinear physical response around the current iteration point. The resulting linear expression is used to guide the subsequent MP decision rather than to replace the original nonlinear physical model.

Traditional Benders decomposition relies on strong duality in a linear or convex continuous subproblem to derive valid analytical cuts. Here, discrete topology changes and

continuous SFCL equivalent series resistances map to a nonconvex AC-network response, so standard cuts cannot be obtained in the same manner. Rigorous nonconvex Benders methods instead require valid relaxations or globally valid cuts together with explicit regularity assumptions [23].

Because the nonlinear physical-verification subproblem does not provide the exact dual information or globally valid relaxations required by those methods, the proposed procedure uses local finite-difference sensitivities only as surrogate guidance coefficients. The resulting constraints are not globally valid supporting hyperplanes. The procedure is therefore classified as a simulation-guided heuristic and does not claim global convergence or global optimality for the original nonconvex MINLP problem.

For a discrete topology variable, x_l, the local response is evaluated by toggling the state of branch l while holding the other variables fixed. For a closed branch changed from $x_l = 1$ to $x_l = 0$, $\Delta x_l = -1$ and the signed finite-change coefficient is:

$$S_{i,l}^{x,k} = \frac{I_{\mathrm{sc},i}^{\mathrm{open},l} - I_{\mathrm{sc},i}^{(k)}}{-1} = I_{\mathrm{sc},i}^{(k)} - I_{\mathrm{sc},i}^{\mathrm{open},l}, \tag{21}$$

where $I_{\mathrm{sc},i}^{(k)}$ is the current at the iteration-k reference plan and $I_{\mathrm{sc},i}^{\mathrm{open},l}$ is the current obtained after opening only branch l at that reference plan. This is a finite state-change coefficient for the binary variable, not an exact analytical derivative.

For continuous SFCL resistance R_l, a forward finite difference is evaluated at iteration k using a small perturbation ΔR_l:

$$S_{i,l}^{R,k} = \frac{I_{\mathrm{sc},i}\left(x^{(k)}, R^{(k)} + \Delta R_l e_l\right) - I_{\mathrm{sc},i}\left(x^{(k)}, R^{(k)}\right)}{\Delta R_l}, \tag{22}$$

where e_l is the unit vector whose l-th component is one, so the perturbation $\Delta R_l e_l$ changes only branch l; all remaining topology and resistance variables are fixed at their iteration-k values. The resulting coefficient is a local finite-difference approximation.

Based on this sensitivity matrix, a local linear sensitivity-guidance constraint is constructed at the current iteration point (x^k, R^k) using a first-order Taylor expansion. If the SP detects that the short-circuit current at node i exceeds the safety threshold $I_{limit,i}$, the new trial solution (x, R) in the subsequent iteration must satisfy:

$$I_{\mathrm{sc},i}^{(k)} + \sum_{l \in \Omega_L} S_{i,l}^{x,k}(x_l - x_l^{(k)}) + \sum_{l \in \Omega_L} S_{i,l}^{R,k}(R_l - R_l^{(k)}) \le I_{\mathrm{limit},i} + \zeta, \tag{23}$$

where ζ is a violation slack variable introduced to preserve the numerical feasibility of the MP during the iterative process, and a penalty is assigned to ζ in the objective function. For convenience in solving the MP as a MILP, the constant terms are moved to the right-hand side of the inequality, yielding:

$$\sum_{l \in \Omega_L} S_{i,l}^{x,k} x_l + \sum_{l \in \Omega_L} S_{i,l}^{R,k} R_l - \zeta \le I_{\mathrm{limit},i} - I_{\mathrm{sc},i}^{(k)} + \sum_{l \in \Omega_L} S_{i,l}^{x,k} x_l^{(k)} + \sum_{l \in \Omega_L} S_{i,l}^{R,k} R_l^{(k)}, \tag{24}$$

This inequality transfers local information between the topology and SFCL-resistance decisions in the MP and the nonlinear short-circuit response. When a nodal violation is detected, the constraint supplies a local direction for changing sensitive branch-status or resistance variables. The nonlinear short-circuit model is recalculated for every new candidate; final feasibility is determined by that calculation rather than by the local linear constraint.

3.3. Iterative Convergence Criterion

The termination of the sensitivity-assisted Benders-type procedure is evaluated using two practical criteria: short-circuit feasibility and objective-value stability. During each iteration, the MP provides the best candidate scheme under its current linear constraints

and accumulated local sensitivity-guidance constraints. The SP then recalculates the short-circuit currents using the nonlinear physical model. The first criterion determines whether the candidate scheme satisfies the short-circuit-current limits, while the second determines whether the objective value has stabilized between successive iterations. These criteria define the numerical termination rule used in this study and should not be interpreted as proof of global convergence or global optimality.

The primary prerequisite for termination is satisfaction of the prescribed current limit. Let $\Delta I_{\max}^{(k)}$ denote the maximum nonnegative current violation at iteration k. The currents and limits used in this convergence test are expressed on the same per-unit base, and $\epsilon_1 = 0.01$ p.u. is the numerical feasibility tolerance:

$$\Delta I_{\max}^{(k)} = \max\left\{0, \max_{i \in \Omega_B}\left[I_{\mathrm{sc},i}^{(k)} - I_{\mathrm{limit},i}\right]\right\} \le \epsilon_1, \tag{25}$$

where Ω_B is the set of constrained nodes in the system and $I_{\mathrm{limit},i}$ is the short-circuit-current security limit of node i. Only when the above condition is satisfied does the algorithm proceed to the objective-stability check. If the short-circuit-feasibility condition is not satisfied, new local sensitivity-guidance constraints are generated and added to the MP.

After short-circuit feasibility is achieved, the change in the objective function between two successive iterations is used as a practical stability indicator. Because the local sensitivity-guidance constraints are constructed locally for a nonconvex physical model, monotonic improvement of the objective value and global optimality are not assumed. The relative change in the objective function is evaluated using the original criterion:

$$\left|\frac{F^{(k)} - F^{(k-1)}}{F^{(k)}}\right| < \epsilon_2, \tag{26}$$

where $F^{(k)}$ is the comprehensive cost value of the MP at iteration k and ϵ_2 is the prescribed objective-stability tolerance. In the numerical implementation, ϵ_2 is set to 10^{-4}. This value is used as a termination tolerance for detecting stabilization of the objective sequence rather than as an optimality-gap certificate.

Algorithm 1 terminates when both the short-circuit-feasibility criterion in Equation (25) and the objective-stability criterion in Equation (26) are satisfied. The output is therefore referred to as the final short-circuit-feasible planning scheme obtained under the prescribed numerical tolerances, rather than a proven global optimum of the original nonconvex problem.

Algorithm 1 Coordinated Suppression Strategy Based on a Sensitivity-Assisted Benders-Type Procedure

procedure Sensitivity_Assisted_Benders_Type_Procedure
Initialize: Iteration index $k \leftarrow 1$, previous objective value $F^{(0)} \leftarrow +\infty$, and maximum iteration number $k_{\max}$.
Pre-calculate the candidate branch set Ω_L based on topological analysis.
while $k \le k_{\max}$ and the termination criteria are not met **do**
    // Phase 1: Master Problem (Discrete Topology & Impedance Investment)
    Solve the MILP master problem to determine the current candidate grid topology $x^{(k)}$ and SFCL equivalent series resistance $R^{(k)}$.
    Record the current master-problem objective value: $F^{(k)} \leftarrow F_{MP}^{(k)}$.
    // Phase 2: Physical Verification Subproblem (AC Short-Circuit Model)
    Update the network admittance matrix Y_{bus} using $(x^{(k)}, R^{(k)})$.
    for each open branch $(x_l = 0)$ **do**
        Apply the virtual minimal conductance G_{open} as a numerical regularization parameter to reduce potential ill-conditioning during topology updates.
    end for
    Execute the AC short-circuit calculation to obtain the node currents $I_{\mathrm{sc},i}^{(k)}$.

Algorithm 1 *Cont.*

Identify the maximum short-circuit-current violation: $\Delta I_{max}^{k} \leftarrow \max\{0, \max_{i\in\Omega_B}[I_{sc,i}^{(k)} - I_{limit,i}]\}$.
// Phase 3: Feasibility Check and Guidance-Constraint Generation
if $\Delta I_{max}^{(k)} \le \epsilon_1$ **then** ▷ Short-Circuit Feasibility Achieved
  if $|(F^{(k)} - F^{(k-1)})/F^{(k)}| < \epsilon_2$ **then** ▷ Objective-Value Stability Achieved
    return the final short-circuit-feasible scheme $(x^*, R^*) \leftarrow (x^{(k)}, R^{(k)})$.
  end if
else
  for each overloaded node i **do**
    Calculate the local finite-difference sensitivities $S_{i,l}^{x,k}$ and $S_{i,l}^{R,k}$ based on the physical short-circuit model.
    Generate a local sensitivity-guidance constraint and add it to the MP.
  end for
end if
Update the iteration index: $k \leftarrow k + 1$.
end while
end procedure

4. Short-Circuit Risk Assessment Model for the Power Grid Based on Fuzzy Comprehensive Evaluation

4.1. Principles of the Fuzzy Comprehensive Evaluation Method

Because current-limiting effectiveness, bus-voltage deviation, equipment investment, and network loss have different dimensions and preference directions, fuzzy comprehensive evaluation is used to compare completed short-circuit-feasible plans on a common scale. The evaluation is a post-optimization ranking step and does not alter the planning decisions.

This section first establishes the basic logical units and set system of the evaluation method:

1. Factor set. The factor set A constitutes the indicator framework of the evaluation object, and its mathematical definition is:

$$A = \{x_1, x_2, \ldots, x_n\}, \tag{27}$$

where each element x_i represents a specific evaluation indicator in the evaluation system. When each element x_i represents a specific evaluation indicator. When the indicators include multiple dimensions, they can be classified into a multilevel model. If the set A contains elements with different attributes, it can be divided into several sub-factor sets $A_1, A_2, \ldots, A_s$, where $A_i = x_{i1}, x_{i2}, \ldots, x_{in_i}$, subject to:

$$\left\{\sum_{i=1}^{s} n_i = n,\ \bigcup_{i=1}^{s} A_i = A,\ A_i \cap A_j = \emptyset, \quad \forall i \neq j.\right., \tag{28}$$

where s is the number of sub-factor sets, n_i is the number of indicators in A_i, and n is the total number of indicators. The conditions ensure completeness and prevent overlap; additional nested partitioning can be introduced when a sub-factor set has its own hierarchy.

2. Comment set. The comment set V is a collection of qualitative grades used to describe the performance of the evaluation indicators:

$$V = \{v_1, v_2, \ldots, v_m\}, \tag{29}$$

Here, m is the number of comment grades. The grades are ordered from the most preferred to the least preferred level; this study uses $m = 5$ grades.

The fixed score vector maps the five comment grades from the most preferred to the least preferred level:

$$G = [1.0,\ 0.8,\ 0.6,\ 0.4,\ 0.2]^{\mathrm{T}}, \tag{30}$$

3. Weight set. The weight set characterizes the relative importance of each evaluation indicator and reflects the decision preference among different performance dimensions:

$$W = [w_1, w_2, \ldots, w_n], \tag{31}$$

Each nonnegative weight w_i corresponds to indicator x_i in the factor set A and represents its relative importance. The weight vector is normalized as follows:

$$w_i \geq 0, \qquad \sum_{i=1}^{n} w_i = 1, \tag{32}$$

In a multilevel evaluation model, the weights can be allocated hierarchically to represent the relative priorities of the global security objective and local operating requirements.

Based on the established set systems, the actual physical state of each indicator is represented by its membership degrees relative to the evaluation grades. This is implemented by constructing the fuzzy relation matrix R:

$$R = \begin{bmatrix} r_{11} & r_{12} & \cdots & r_{1m} \\ r_{21} & r_{22} & \cdots & r_{2m} \\ \vdots & \vdots & \ddots & \vdots \\ r_{n1} & r_{n2} & \cdots & r_{nm} \end{bmatrix}, \tag{33}$$

Here, r_{ij} is the membership degree of indicator x_i in comment grade v_j, with $i = 1, \ldots, n$ and $j = 1, \ldots, m$. The membership vector for indicator i is $r_i = [r_{i1}, \ldots, r_{im}]$, where $r_{ij} \geq 0$ and $\sum_{j=1}^{m} r_{ij} = 1$.

Once the single-factor membership information is obtained, the weight vector and fuzzy relation matrix are synthesized to give the comprehensive membership vector S:

$$S = W \cdot R = [s_1, s_2, \ldots, s_m], \tag{34}$$

Each s_j is the aggregated membership degree of the evaluated scheme in comment grade v_j, and $\sum_{j=1}^{m} s_j = 1$ after normalization.

Finally, defuzzification is performed through an inner-product operation to obtain the comprehensive evaluation score Q:

$$Q = S \cdot G = \sum_{j=1}^{m} s_j g_j, \tag{35}$$

where g_j is the fixed scalar score assigned to grade v_j in G. The comprehensive score Q compares candidate schemes under the same indicators, membership functions, and preference weights; it does not replace the short-circuit-feasibility check.

4.2. First-Level Evaluation of Current-Limiting Effect Considering Urgency

From a physical perspective, the thermal effect and electrodynamic stress imposed on equipment increase approximately with the square of current magnitude. The urgency index of station j is therefore defined as:

$$\kappa_j = \left(\frac{I^0_{\mathrm{sc},j}}{I_{0,j}} \right)^2, \tag{36}$$

where $I^0_{\mathrm{sc},j}$ is the initial calculated short-circuit current at station j and $I_{0,j}$ is the rated interrupting current of the corresponding circuit breaker.

The symbol κ_j denotes current-limiting urgency and is distinct from the iteration index k used in Section 2. When $\kappa_j \geq 1$, the initial current reaches or exceeds the rated interrupting capacity and the station receives the highest urgency. Lower values are assigned to warning groups according to the remaining interrupting margin.

The monitored stations are divided into Y mutually disjoint urgency groups. For station set Ω_B, group y is $B_y = \{j \in \Omega_B \mid \gamma_{y-1} \leq \kappa_j < \gamma_y\}$, where γ_{y-1} and γ_y are its interval bounds. The groups satisfy $B_y \cap B_z = \emptyset$ for $y \neq z$ and $\bigcup_{y=1}^{Y} B_y = \Omega_B$. A group nearer to or beyond the interrupting limit receives a higher priority.

After grouping, the analytic hierarchy process (AHP) pairwise-comparison matrix $A_{\text{seg}} = (a_{yz}) \in \mathbb{R}^{Y\times Y}$ is constructed according to urgency. If group y is more urgent than group z, then $a_{yz} \geq 1$ and $a_{zy} = 1/a_{yz}$. The normalized principal eigenvector gives $W_{\text{seg}} = [w_1, \ldots, w_Y]$, where $\sum_{y=1}^{Y} w_y = 1$. Within group B_y, τ_j is the normalized station weight, with $\sum_{j\in B_y} \tau_j = 1$.

To avoid evaluating the current-limiting effect using an absolute current-reduction scale that varies with the initial short-circuit level of each test system, the set of stations requiring current suppression is first defined as:

$$\Omega_B^+ = \{j \in \Omega_B \mid I_{\text{sc},j}^0 > I_{0,j}\}, \tag{37}$$

where Ω_B^+ is the set of stations whose initial current exceeds the corresponding interrupting limit. For each station, the actual and minimum required reductions are:

$$\Delta I_{\text{sc},j} = \max\left(0, I_{\text{sc},j}^0 - I_{\text{sc},j}^{\text{opt}}\right), \tag{38}$$

$$\Delta I_{\text{sc},j}^{\text{req}} = \max\left(0, I_{\text{sc},j}^0 - I_{0,j}\right), \tag{39}$$

where $I_{\text{sc},j}^{\text{opt}}$ is the post-planning current. The current-limiting achievement indicator is the ratio of the urgency-weighted actual reduction to the urgency-weighted minimum required reduction:

$$\lambda_{\text{sc}} = \frac{\sum_{y=1}^{Y} w_y \sum_{j\in B_y\cap\Omega_B^+} \tau_j \Delta I_{\text{sc},j}/I_{0,j}}{\sum_{y=1}^{Y} w_y \sum_{j\in B_y\cap\Omega_B^+} \tau_j \Delta I_{\text{sc},j}^{\text{req}}/I_{0,j}}, \tag{40}$$

Within every nonempty $B_y \cap \Omega_B^+$, the station weights are renormalized so that $\sum_{j\in B_y\cap\Omega_B^+} \tau_j = 1$. Thus, $\lambda_{\text{sc}} = 1$ means that the weighted minimum required reduction is exactly achieved, $\lambda_{\text{sc}} > 1$ represents an additional current margin, and $\lambda_{\text{sc}} < 1$ represents incomplete achievement. If $\Omega_B^+ = \emptyset$, λ_{sc} is defined as 1 because the initial system has no over-limit station.

Short-circuit feasibility and fuzzy preference are deliberately separated. Short-circuit feasibility requires $I_{\max} \leq I_{\text{limit}}$ and is checked before ranking. A short-circuit-feasible plan does not automatically receive a full current-limiting score; the full score is assigned only when the calculated λ_{sc} reaches the highest membership interval.

Finally, the calculated current-limiting indicators are converted into membership degrees through the membership functions, forming the fuzzy relation matrix R_{sc}. This allows the current-limiting performance of different suppression schemes to be evaluated on the same comment scale while preserving the differences among urgency groups.

4.3. Fuzzy Comprehensive Evaluation Model for Short-Circuit Current Limitation Measures

Evaluating short-circuit current limitation schemes is a multi-criteria decision-making problem in which the indicators differ in physical dimensions and relative importance. In this study, a multilevel fuzzy comprehensive evaluation system is constructed using

four indicators: current-limiting achievement, steady-state bus-voltage deviation, equipment investment, and relative system network-loss increase.

1. The current-limiting achievement indicator λ_{sc} is defined in Equation (40). It compares the urgency-weighted actual reduction with the minimum reduction required by the breaker interrupting limits and is used only to rank feasible plans; it is not a transient- or dynamic-stability index.
2. The steady-state bus-voltage deviation indicator λ_U evaluates the voltage-profile influence of the reconfigured grid by accumulating the deviations of the monitored bus voltages from the rated voltage:

$$\lambda_U = \sum_{i \in \beta} W_{U,i} |U_i - U_N|, \tag{41}$$

where β is the set of buses included in the voltage assessment, $W_{U,i}$ is the normalized voltage weight of bus i, U_i is the bus-voltage magnitude in per unit, and $U_N = 1.0$ p.u. is the rated-voltage reference. A smaller λ_U indicates that the steady-state voltage profile is closer to the rated operating point. The voltage feasibility of each bus is additionally checked against its prescribed lower and upper operating limits; therefore, λ_U is used for ranking feasible schemes rather than replacing the bus-voltage constraints.

3. The equipment-investment indicator λ_D measures the one-time construction cost of the current-limiting project, including the purchase of newly installed current-limiting devices, circuit-breaker interrupting-capacity upgrades, and construction associated with grid-topology adjustment:

$$\lambda_D = \sum_{i \in \Theta} M_i, \tag{42}$$

where Θ is the set of retrofitted or newly installed items in the plan and M_i is the cost of item i, expressed in million Chinese yuan (CNY). The indicator compares the one-time investment requirements of different technical routes.

4. The relative system network-loss increase indicator λ_{loss} describes the percentage increase in active network loss after implementation of a current-limiting scheme:

$$\lambda_{\text{loss}} = 100\% \times \frac{\max\left(0, P_{\text{loss}}^{\text{opt}} - P_{\text{loss}}^{0}\right)}{P_{\text{loss}}^{0}}, \tag{43}$$

where P_{loss}^{0} and P_{loss}^{opt} are the total active network losses under the initial and optimized operating conditions, respectively. A scheme that reduces the network loss is assigned $\lambda_{loss} = 0$. Expressing the loss variation as a percentage of the initial loss avoids dependence on the absolute size of a test system and improves the comparability of the indicator across operating scenarios.

Based on the indicator set $X = \{\lambda_{sc}, \lambda_U, \lambda_D, \lambda_{loss}\}$, each physical quantity is mapped to its membership degrees with respect to the comment set $V = \{v_1, v_2, v_3, v_4, v_5\}$.

For traceable comparison under the same operating condition, each indicator is mapped to the five grades using piecewise-linear membership functions anchored to specified physical or economic thresholds. Adjacent grades are connected by linear interpolation, endpoint values are assigned outside the threshold range, and every membership vector is normalized to sum to one. The threshold and weight choices remain explicit planning preferences.

For cost-type indicators, where a lower value is preferred, including λ_U, λ_D, and λ_{loss}, let $C = (c_1, c_2, c_3, c_4)$ be the threshold vector satisfying $c_1 < c_2 < c_3 < c_4$. The membership functions are:

$$\mu_{v_1}(x) = \begin{cases} 1, & x \le c_1, \\ \dfrac{c_2 - x}{c_2 - c_1}, & c_1 < x < c_2,, \\ 0, & x \ge c_2. \end{cases} \tag{44}$$

$$\mu_{v_k}(x) = \begin{cases} \dfrac{x - c_{k-1}}{c_k - c_{k-1}}, & c_{k-1} < x \le c_k, \\ \dfrac{c_{k+1} - x}{c_{k+1} - c_k}, & c_k < x < c_{k+1}, \\ 0, & \text{otherwise}, \end{cases} \quad k \in \{2, 3, 4\}, \tag{45}$$

$$\mu_{v_5}(x) = \begin{cases} 0, & x \le c_4, \\ \dfrac{x - c_4}{x_{\max} - c_4}, & c_4 < x < x_{\max},, \\ 1, & x \ge x_{\max}. \end{cases} \tag{46}$$

The current-limiting achievement indicator λ_{sc} is a benefit-type indicator, for which a larger value is preferred. Its descending threshold vector (c_1, c_2, c_3, c_4) is converted to the cost-type form by setting $t = -x$ and $(\tilde{c}_1, \tilde{c}_2, \tilde{c}_3, \tilde{c}_4) = (-c_1, -c_2, -c_3, -c_4)$ and applying Equations (44)–(46) to t. For terminal grades, $x_{\max} = c_4 + (c_4 - c_3)$ for a cost-type indicator and $x_{\min} = \max[0, c_4 - (c_3 - c_4)]$ for a nonnegative benefit-type indicator.

The revised thresholds are selected according to the physical meanings of the normalized indicators rather than fitted to the ranking of a particular algorithm. For λ_{sc}, a value of 1.0 represents completion of the required weighted reduction, while 1.2 represents a 20% additional current-limiting margin. For λ_U, the thresholds represent increasing average deviations from the 1.0 p.u. rated-voltage reference and retain the 0.05 p.u. operating-boundary scale. For λ_{loss}, the thresholds represent relative loss increases of 1%, 5%, 10%, and 20%, thereby avoiding the saturation produced by absolute-MW thresholds in systems of different sizes. The threshold definitions and their physical interpretations for the four evaluation indicators are summarized in Table 1.

Table 1. Threshold Definitions for Evaluation Indicators.

λ_{sc} (dimensionless)	$c_1 = 1.20$, $c_2 = 1.00$, $c_3 = 0.80$, $c_4 = 0.60$	Ratio of the urgency-weighted actual current reduction to the minimum reduction required by the interrupting limits
λ_U (p.u.)	$c_1 = 0.005$, $c_2 = 0.015$, $c_3 = 0.030$, $c_4 = 0.050$	Weighted average absolute deviation from the 1.0 p.u. rated-voltage reference
λ_D (10^6 CNY)	$c_1 = 500$, $c_2 = 1000$, $c_3 = 2000$, $c_4 = 4000$	Marginal investment levels of the candidate current-limiting measures
λ_{loss} (%)	$c_1 = 1$, $c_2 = 5$, $c_3 = 10$, $c_4 = 20$	Percentage increase in active network loss relative to the initial operating condition

The four criterion weights are retained as predefined planning preferences. For transparent AHP representation, let $A_W = (a_{ij}) \in \mathbb{R}^{4\times4}$ with $a_{ij} = w_i/w_j$. This construction is reciprocal and perfectly consistent, so $A_W W = 4W$, $\lambda_{\max} = 4$, and the consistency ratio (CR)

is zero. The zero CR follows mathematically from the weight-consistent construction and is not independent empirical validation of the preferences.

$$A_W = \begin{bmatrix} 1 & \frac{9}{4} & \frac{9}{4} & 3 \\ \frac{4}{9} & 1 & 1 & \frac{4}{3} \\ \frac{4}{9} & 1 & 1 & \frac{4}{3} \\ \frac{1}{3} & \frac{3}{4} & \frac{3}{4} & 1 \end{bmatrix}, \tag{47}$$

The normalized principal eigenvector of A_W is exactly the adopted weight vector:

$$W = [0.45, 0.20, 0.20, 0.15], \tag{48}$$

For an order-n AHP matrix, $\lambda_{\max}$ is the maximum eigenvalue, $CI = (\lambda_{\max} - n)/(n-1)$ is the consistency index, RI is the random consistency index, and $CR = CI/RI$ is the consistency ratio. Here, $n = 4$ and $RI = 0.90$, giving:

$$A_W W = 4W, \qquad \lambda_{\max} = 4, \qquad CI = \frac{\lambda_{\max} - 4}{4 - 1} = 0, \qquad CR = \frac{CI}{RI} = 0, \tag{49}$$

All comprehensive scores were recalculated using the unified rule above. Because the adopted baseline weight vector remains $W = [0.45, 0.20, 0.20, 0.15]$, the recalculated numerical values are identical to those reported in the case-study tables. The resulting rankings are interpreted only under this stated preference, and the weight vector is not claimed to be unique.

For indicator j, let r_j be its 1×5 membership row vector and let G be the 5×1 grade-score vector. The scalar indicator score is $d_j = r_j G$. The same aggregation rule is used for every method and case:

$$d_j = r_j G, \qquad Q = \sum_{j=1}^{4} w_j d_j = W \begin{bmatrix} d_1 & d_2 & d_3 & d_4 \end{bmatrix}^{\mathrm{T}}, \tag{50}$$

A larger Q denotes a more favorable ranking under the adopted membership thresholds and baseline weights. The value of Q ranks completed short-circuit-feasible planning schemes and does not replace the short-circuit verification or feed back into the optimization search.

5. Case Study

5.1. Modified CSEE-VS-66 System Under Standard Multi-DC Operation

To verify the effectiveness of the proposed coordinated optimization strategy, simulations were conducted on an improved CSEE-VS-66 system [24]. The original topology was expanded by integrating a second LCC-HVDC infeed at bus B02, complementing the existing DC infeed at bus B21. The topology of the modified CSEE-VS-66 system is shown in Figure 2. Detailed line, transformer, generator, renewable-energy, load, and reactive-power-compensation parameters of this system are provided in Appendix A.

The system base parameters are defined to ensure physical and mathematical consistency throughout the optimization process. The base power is set to $S_B = 1000$ MVA, and the base voltage of the main transmission network is $U_N = 525$ kV. Consequently, the base impedance used for per-unit conversion is calculated as:

$$Z_B = \frac{U_N^2}{S_B} \approx 275.62\,\Omega, \tag{51}$$

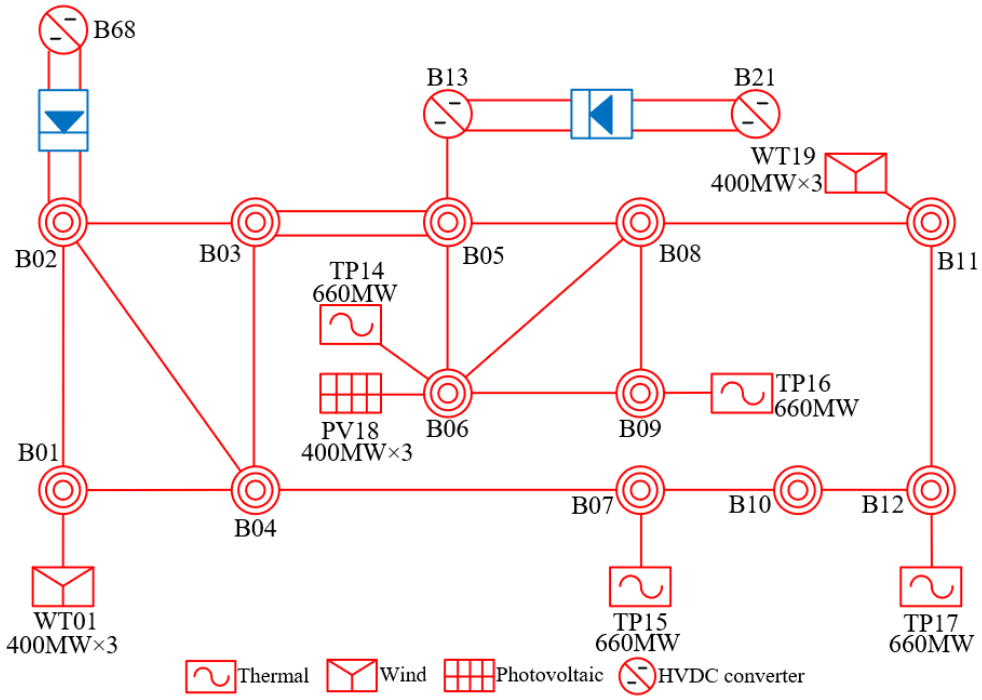


Figure 2. Modified CSEE-VS-66 System.

During the iterations of the sensitivity-assisted Benders-type procedure, all continuous resistance variables are calculated in per-unit values. After the final planning scheme is obtained, the SFCL equivalent series resistance is converted to ohms using Z_B. The upper limit of the injected SFCL equivalent series resistance is set to $R_{max} = 0.5$ p.u.

In the numerical implementation, $R_{min} = 0.001$ p.u. and $R_{max} = 0.5$ p.u.; on the 525 kV, 1000 MVA base, these values correspond to approximately 0.276 Ω and 137.81 Ω, respectively. The lower bound is both the minimum installed resistance enforced by the planning model and the numerical resolution used for candidate resistance settings. The upper bound is a nonbinding search limit in the reported cases. These are planning-model bounds rather than universal SFCL ratings; manufacturer-specific trigger, thermal-duty, recovery, and protection-coordination limits must be imposed before engineering implementation.

The modified benchmark retains 66 buses. Seven 525 kV buses, namely B03, B04, B05, B08, B09, B06, and B14, are monitored in the short-circuit-current optimization. The planning search uses 17 candidate 525 kV branches for line opening and SFCL allocation. The short-circuit-current limit of every monitored 525 kV bus is set to 63.0 kA. For post-optimization contingency verification, the configured component set contains 24 line records at 525 kV, 13 generator records, and two LCC-HVDC bipoles.

All four methods were executed independently on the same 64-bit Windows laptop computer (ROG Zephyrus G16) equipped with an Intel Core Ultra 9 185H processor, 32 GB of RAM, and an NVIDIA GeForce RTX 4060 Laptop GPU. MATLAB R2024a was used to implement the optimization algorithms and manage data exchange, while PSD-BPA SCCP 2.8.6-SP1 was used for the physical short-circuit calculations. The optimization and BPA calculations were executed on the CPU without explicit GPU acceleration. Reported runtimes are wall-clock times for one optimization run and exclude the subsequent selected single-component-outage screening. The common simulation and algorithm parameters are summarized in Table 2.

Table 2. Common simulation and algorithm parameters.

Parameter	Value
Base power S_B	1000 MVA
Main-grid base voltage U_N	525 kV
Base impedance Z_B	275.62 Ω
Maximum SFCL equivalent series resistance	0.5 p.u. (137.81 Ω)
Maximum opened branches	2 (4 for Onlyswitching)
Line-opening cost	500 (10^6 CNY)/line
SFCL variable-cost coefficient	10,000 (10^6 CNY)/p.u.
Minimum installed SFCL equivalent series resistance	0.001 p.u. (0.276 Ω)

Four solution methods are compared using the same monitored buses, candidate branches, cost coefficients, current limit, and BPA short-circuit model. Their method-specific settings are as follows:

- Proposed coordinated method. The maximum number of sensitivity-assisted Benders-type iterations is 30. The master problem jointly determines line states and continuous SFCL equivalent series resistances, and the subproblem recalculates the nonlinear short-circuit currents.
- Mixed-integer genetic algorithm (MIGA). The population size is 40, the maximum number of generations is 50, the maximum number of stall generations is 15, the elite count is 4, and the crossover fraction is 0.8. The function and constraint tolerances are 10^{-4} and 10^{-6}, respectively. The SFCL equivalent series resistance resolution is 0.001 p.u.
- SFCL-only method. All candidate branches remain closed, and only their SFCL equivalent series resistances are optimized. The maximum number of iterations is 30.
- Switching-only method. All SFCL equivalent series resistances are fixed at zero, and only the branch-status variables are optimized over the same 17-branch candidate set. Up to four branch openings are permitted to avoid imposing an artificial infeasibility on this single-measure benchmark.

Under the standard multi-DC operating condition, the initial maximum short-circuit current is 65.16 kA at bus B05, exceeding the 63.0 kA limit by 2.16 kA. The final schemes and computational results are summarized in Table 3.

Table 3. Short-circuit-current suppression schemes for the modified CSEE-VS-66 system under the standard multi-DC condition.

Method	Final Planning Scheme	Cost (10^6 CNY)	I_{max}	Runtime	Iterations/Guidance Constraints	BPA Evaluations
Proposed method	Open B04–B07; SFCL on B06–B05, $R = 0.3665$ Ω.	513.298	62.96 kA	29.216 s	3/1	39
MIGA	Open B07–B10; Open B08–B11.	1000.000	57.49 kA	421.794 s	16/0	576
SFCL only	SFCL on B06–B05, $R = 13.9875$ Ω; SFCL on B04–B07, $R = 2.1033$ Ω.	583.804	63.00 kA	102.963 s	5/4	141
Switching only	Open B06–B05; Open B05–B03-1.	1000.0	62.54 kA	29.047 s	2/1	36

All four reruns satisfy the 63.0 kA short-circuit-current limit and are retained in the comparative evaluation. The proposed coordinated plan has the lowest nominal investment cost: 12.08% below SFCL-only and 48.67% below switching-only. The switching-only plan attains the highest fuzzy score (0.8266), while the proposed, MIGA, SFCL-only, and switching-only scores are 0.7557, 0.6800, 0.7639, and 0.8266, respectively. Runtime and BPA evaluations are supplementary computational information and do not enter the comprehensive score.

Figure 3 directly compares the seven monitored-bus currents before and after the corrected coordinated rerun. The maximum current decreases from 65.16 kA at B05 to 62.96 kA, and every plotted value remains at or below the 63.0 kA limit after optimization. The plot establishes short-circuit-current-limit compliance for this case.

Table 4 presents the fuzzy comprehensive evaluation results for the standard multi-DC condition across current-limiting effect, voltage deviation, equipment investment, and network loss.

Table 4. Fuzzy evaluation results for the standard multi-DC condition.

Evaluation Indicator d_j	Weight W	Proposed Method	MIGA	SFCL Only	Switching Only
d_1	0.45	0.8185	1.0000	0.8000	1.0000
d_2	0.20	0.7924	0.2000	0.9029	0.9000
d_3	0.20	0.9947	0.8000	0.9665	0.8000
d_4	0.15	0.2000	0.2000	0.2000	0.2439
Comprehensive Evaluation Priority	1	0.7557	0.6800	0.7639	0.8266

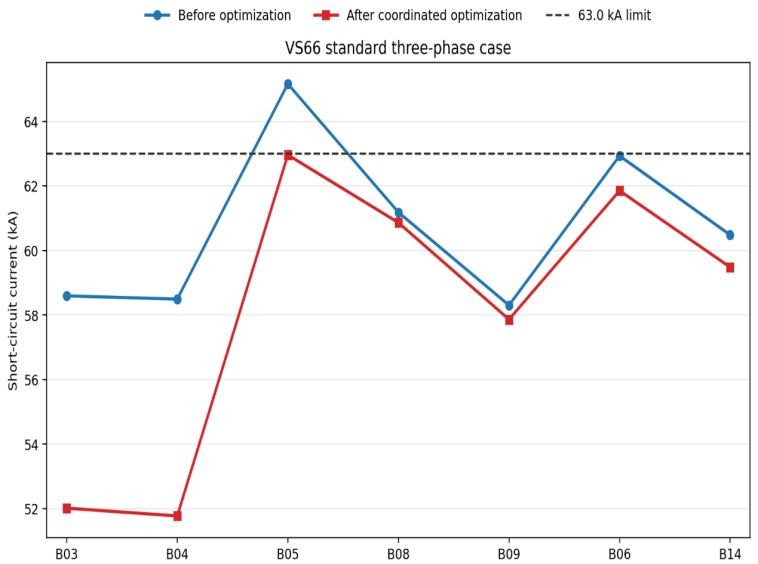


Figure 3. Short-circuit-current levels before and after coordinated optimization under the standard multi-DC condition.

The fuzzy scores are 0.7557, 0.6800, 0.7639, and 0.8266 for the proposed, MIGA, SFCL-only, and switching-only plans, respectively. The switching-only plan ranks first under the stated weights, whereas the proposed plan has the lowest nominal cost and modifies only two corridors. These results show that short-circuit-current compliance, economic cost, computational effort, and preference-based ranking describe different attributes and should be interpreted separately.

A selected single-component-outage short-circuit-current screening was conducted for the corrected coordinated scheme. The screening comprised 24 single-line outages at the 525 kV level, 13 single-generator outages, and two LCC-HVDC bipole outages, resulting in 39 selected cases. The results are summarized in Table 5.

Table 5. Selected single-component-outage short-circuit-current screening results for the standard multi-DC condition; pass criterion: $I_{max} \leq 63.0$ kA.

Contingency Type	Selected Cases	Largest Current	Representative Worst Case	Cases with $I_{max} \leq 63.0$ kA
525 kV line outage	24	62.96 kA	B13-B05-1	24/24
Generator outage	13	62.66 kA	GEN-WT19-01	13/13
HVDC bipole outage	2	62.96 kA	HVDC-B21-B13 bipole	2/2

All 39 selected cases satisfy the 63.0 kA short-circuit-current criterion. The category maxima are 62.96 kA for line outages, 62.66 kA for generator outages, and 62.96 kA for HVDC bipole outages. These values describe only the selected-outage current screening. Planned-line reclosure, SFCL non-insertion, and broader contingency-state operating criteria are outside the tested set.

From a planning perspective, the coordinated solution requires only one topology adjustment and one SFCL installation with a relatively small equivalent series resistance. This limits both the number of modified corridors and the required SFCL capacity. Nevertheless, practical implementation still requires project-specific checking of switching arrangements, equipment ratings, and operating procedures. The case-study conclusions are therefore restricted to planning-oriented short-circuit-current suppression and steady-state indices supported by the benchmark data.

5.2. Modified CSEE-VS-66 System Under High-Load Operation

To further examine the adaptability of the proposed strategy under a more severe operating condition, the high-load operating point of the modified CSEE-VS-66 system is considered. The system topology, monitored buses, candidate branches, cost coefficients, per-unit conversion, computing platform, and short-circuit-current limit are identical to those specified in Section 4.1 and are therefore not repeated here.

Under this operating condition, the initial short-circuit currents at buses B05 and B06 are 67.19 kA and 64.72 kA, respectively, both exceeding the prescribed limit of 63.0 kA. The initial maximum violation is therefore 4.19 kA, which makes this condition more demanding than the standard multi-DC operating condition considered in Section 4.1.

The four rerun schemes are summarized in Table 6. Cost is expressed in 10^6 CNY. Runtime and BPA evaluations refer to the optimization process and exclude the subsequent selected-outage screening; they are supplementary computational information and are not components of the comprehensive score. Short-circuit-current compliance and post-optimization preference scores are reported using the same comparison basis for all four methods.

Table 6. Short-circuit-current suppression schemes for the modified CSEE-VS-66 system under the high-load condition.

Method	Final Planning Scheme	Cost (10^6 CNY)	I_{max}	Runtime	Iterations/Guidance Constraints	BPA Evaluations
Proposed method	Open B04–B07; SFCL on B06–B05, $R = 15.1664\ \Omega$.	1050.265	61.33 kA	29.170 s	3/1	39
MIGA	Open B06–B05; Open B05–B08.	1000.0	59.67 kA	980.822 s	40/0	1349
SFCL only	SFCL on B06–B05, $R = 21.3988\ \Omega$; SFCL on B04–B07, $R = 10.4841\ \Omega$.	1156.768	62.80 kA	52.194 s	3/2	71
Switching only	Open B06–B05; Open B04–B07; Open B05-B03-1.	1500.0	61.11 kA	27.996 s	2/1	36

All four high-load three-phase reruns satisfy the 63.0 kA short-circuit-current limit. The proposed scheme reduces the maximum current from 67.19 to 61.33 kA, a reduction of 5.86 kA (8.72%), and retains a 1.67 kA current margin. Its cost is 9.21% lower than SFCL-only and 29.98% lower than switching-only. MIGA is 4.79% cheaper than the proposed scheme when the proposed cost is used as the denominator. The proposed scheme obtains the highest fuzzy score, 0.8180, only slightly above SFCL-only (0.8132) and switching-only (0.8106), so the methods should be regarded as close under the stated weights.

Figure 4 compares B03, B04, B05, B08, B09, B06, and B14 in the stated order. Before optimization, B05 and B06 reach 67.19 and 64.72 kA; after the corrected coordinated rerun, they decrease to 61.33 and 55.72 kA, respectively.

Table 7 presents the fuzzy comprehensive evaluation results for the high-load condition across current-limiting effect, voltage deviation, equipment investment, and network loss.

Table 7. Fuzzy evaluation results for the high-load condition.

Evaluation Indicator d_j	Weight W	Proposed Method	MIGA	SFCL Only	Switching Only
d_1	0.45	1.0000	1.0000	1.0000	1.0000
d_2	0.20	0.9000	0.7314	0.8971	0.8971
d_3	0.20	0.7899	0.8000	0.7686	0.7000
d_4	0.15	0.2000	0.2000	0.2000	0.2748
Comprehensive Evaluation Priority	1	0.8180	0.7863	0.8132	0.8106



Figure 4. Short-circuit-current levels at the seven monitored buses before and after coordinated optimization under the high-load condition.

Under the stated weights, the corrected comprehensive scores are 0.8180, 0.7863, 0.8132, and 0.8106 for the proposed, MIGA, SFCL-only, and switching-only plans. The proposed method is marginally first, but the small gaps indicate comparable multi-criteria performance rather than robust dominance.

A selected single-component-outage short-circuit-current screening was conducted for the corrected coordinated scheme under the high-load three-phase condition. The set contains 24 line outages, 13 generator outages, and two HVDC bipole outages, for 39 selected cases. The corresponding screening results are summarized in Table 8.

Table 8. Selected single-component-outage short-circuit-current screening results for the high-load condition; pass criterion: $I_{max} \leq 63.0$ kA.

Contingency Type	Selected Cases	Largest Current	Representative Worst Case	Cases with $I_{max} \leq 63.0$ kA
525 kV line outage	24	61.34 kA	B09-B06-1	24/24
Generator outage	13	61.10 kA	GEN-WT19-01	13/13
HVDC bipole outage	2	61.33 kA	HVDC-B21-B13 bipole	2/2

All 39 selected cases satisfy the 63.0 kA current criterion. The category maxima are 61.34 kA, 61.10 kA, and 61.33 kA for line, generator, and HVDC outages, respectively. The line-outage maximum is 0.01 kA above the intact value. The result is therefore reported as selected-outage short-circuit-current screening rather than as a non-increase test.

The coordinated scheme combines one branch opening with an SFCL equivalent series resistance of 15.1664 Ω. Compared with the SFCL-only scheme, it avoids 16.7164 Ω of installed equivalent series resistance and costs 9.21% less; compared with switching-only, it opens two fewer branches and costs 29.98% less. The modest fuzzy-score advantage indicates a balanced but preference-dependent result rather than categorical superiority.

To further examine the applicability of the proposed coordinated planning method under an asymmetrical fault condition, the three-phase fault setting was replaced by a single-line-to-ground fault, while the system operating condition, candidate planning measures, and short-circuit current limit were kept unchanged. Before optimization, the single-line-to-ground fault currents at buses B03, B04, B05, B08, B09, B06, and B14 were 59.87, 59.80, 66.18, 56.68, 51.70, 59.84, and 55.57 kA, respectively. The maximum current occurred at bus B05 and exceeded the 63 kA limit by 3.18 kA. The short-circuit-current levels before and after independent optimization under the single-line-to-ground fault condition are compared in Figure 5.

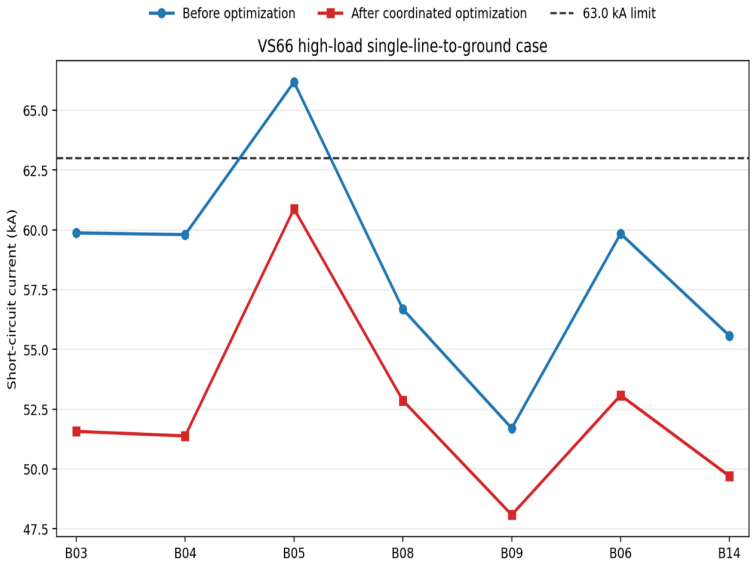


Figure 5. Single-line-to-ground short-circuit currents at the seven monitored buses before and after independent optimization under the high-load condition.

Under the independently solved single-line-to-ground case, the corrected coordinated method converges after three iterations with one guidance constraint. It opens B04–B07 and installs an SFCL equivalent series resistance of 3.8318 Ω on B06–B05; the unrounded value used in the cost calculation is 0.0139024390243902 p.u. The optimized currents at B03, B04, B05, B08, B09, B06, and B14 are 51.57, 51.38, 60.88, 52.86, 48.08, 53.08, and 49.70 kA.

The independently optimized three-phase and single-line-to-ground fault schemes are compared in Table 9.

Table 9. Independently optimized three-phase and single-line-to-ground fault schemes for the modified CSEE-VS-66 system.

Fault type	Final Planning Scheme	Cost (10^6 CNY)	I_{max}	Runtime	Iterations/Guidance Constraints	BPA Evaluations
Three-phase Fault	Open B04–B07; SFCL on B06–B05, $R = 15.1664\ \Omega$.	1050.265	61.33 kA	29.170 s	3/1	39
Single-line-to-ground Fault	Open B04–B07; SFCL on B06–B05, $R = 3.8318\ \Omega$.	639.024	60.88 kA	29.210 s	3/1	39

The three-phase and SLG cases are solved independently. Both converge in three iterations with one guidance constraint and 39 short-circuit evaluations, but they yield different SFCL-resistance decisions because their fault models differ. The asymmetrical case uses the single-line-to-ground option available in the adopted case-study calculation chain. Because a separate zero-sequence data file was not available, this case is reported as a reproducible representative asymmetrical-fault scenario rather than a general validation of every zero-sequence network model.

The single-line-to-ground scheme has indicator scores 1.0000, 0.9057, 0.9444, and 0.2000 and a comprehensive score of 0.8500. Its maximum current is 60.88 kA, below the 63.0 kA limit. The score is used only for post-optimization comparison and does not replace the short-circuit-current criterion. The corresponding fuzzy evaluation results are summarized in Table 10.

Table 10. Fuzzy evaluation results for the independently optimized fault cases.

Evaluation Indicator d_j	Weight W	Three-Phase Fault	Single-Line-to-Ground Fault
d_1	0.45	1.0000	1.0000
d_2	0.20	0.9000	0.9057
d_3	0.20	0.7899	0.9444
d_4	0.15	0.2000	0.2000
Comprehensive Evaluation Priority	1	0.8180	0.8500

All 39 selected SLG outage cases satisfy the 63.0 kA current criterion. The category maxima are 61.26 kA for line outages, 60.79 kA for generator outages, and 60.88 kA for HVDC outages. Because the line-outage maximum exceeds the intact value of 60.88 kA, the result is reported as selected-outage short-circuit-current screening rather than as a non-increase check.

The independent comparison confirms that the planning framework can be re-applied to both a three-phase and a representative asymmetrical fault model. It does not establish that the plan optimized for one fault is automatically valid for the other; a common multi-fault robust plan would require a different joint formulation and is outside the present study.

5.3. Modified CSEE-FS-47 System Under Standard Multi-DC Operation

To further examine the applicability of the proposed coordinated optimization method to a different network structure, an additional case study was conducted using the CSEE-FS-47 system [25]. The system contains 47 key buses, 31 AC transmission lines, 62 transformers, and three ±500 kV HVDC links. Its conventional generation capacity is 5400 MW, compris-

ing five thermal units with a total capacity of 3400 MW and two hydropower units with a total capacity of 2000 MW. The installed wind and photovoltaic capacities are 3150 MW and 3750 MW, respectively, giving a total renewable capacity of 6900 MW and a renewable penetration of 56.1%. The total active and reactive loads are 4852.1 MW and 1528 Mvar, respectively. The topology of the CSEE-FS-47 system is shown in Figure 6. Detailed line, transformer, generator, renewable-energy, load, and reactive-power-compensation parameters of this system are provided in Appendix A.2.

The main AC transmission network is represented by the 525 kV voltage level in the BPA model. Ten buses, namely B01, B02, B03, B04, B05, B06, B07, B08, B10, and B12, are monitored in the short-circuit-current calculation. Eleven 525 kV transmission branches are included in the planning candidate set for line opening and SFCL allocation. The per-unit base, short-circuit-current limit, equipment-cost coefficients, computing platform, and algorithm parameters are identical to those specified in Section 4.1 and are therefore not repeated here. A maximum of three branch openings is permitted for this system.

Under the original operating condition, the maximum three-phase short-circuit current is 64.94 kA, which exceeds the prescribed limit of 63.0 kA by 1.94 kA. The proposed coordinated method and the three comparison methods were independently applied to the same monitored buses, planning candidates, cost coefficients, and BPA short-circuit model. Their final planning schemes and computational results are summarized in Table 11.

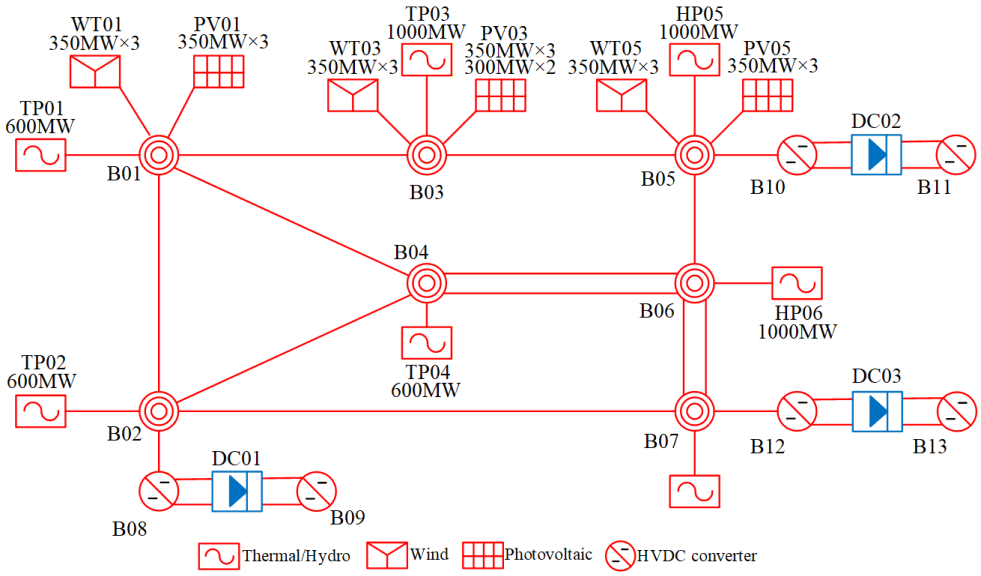


Figure 6. Modified CSEE-FS-47 system.

Table 11. Short-Circuit Current Suppression Schemes for the Modified CSEE-FS-47 System.

Method	Final Planning Scheme	Cost (10^6 CNY)	I_{max}	Runtime	Iterations/Guidance Constraints	BPA Evaluations
Proposed method	SFCL on B03–B05, R = 13.1203 Ω; SFCL on B05–B06, R = 0.7227 Ω.	502.240	63.00 kA	160.561 s	22/20	253
MIGA	Open B03–B05; Open B05–B06.	1000.000	34.91 kA	465.075 s	22/0	734
SFCL only	SFCL on B03–B05, R = 12.0026 Ω; SFCL on B05–B06, R = 1.0785 Ω.	474.599	63.00 kA	278.601 s	20/19	438
Switching only	Open B03–B05; Open B05–B06.	1000.000	34.91 kA	31.387 s	3/2	47

All four CSEE-FS-47 reruns satisfy the 63.0 kA short-circuit-current limit and are retained in the comparative evaluation. The corrected coordinated scheme uses two SFCLs—13.1203 Ω on B03–B05 and 0.7227 Ω on B05–B06—with no line opening, and its maximum current is 63.00 kA.

Among the four compared planning solutions, SFCL-only has the lowest nominal cost: 474.599 × 10^6 CNY, 5.50% below the proposed cost of 502.240 × 10^6 CNY. The proposed plan has the highest comprehensive score, 0.8907, only slightly above the SFCL-only score of 0.8803, because its small voltage-deviation advantage and better loss score offset its slightly lower investment score under the baseline weights. Runtime and BPA evaluations are supplementary only and do not enter Q.

Figure 7 uses B01, B02, B03, B04, B05, B06, B07, B08, B10, and B12. Before optimization, the maximum is 64.94 kA at B05 and B10; after the corrected coordinated rerun, the maximum is 63.00 kA at B05 and B10.

Table 12 presents the fuzzy comprehensive evaluation results for the standard multi-DC condition across current-limiting effect, voltage deviation, equipment investment, and network loss.

Table 12. Fuzzy evaluation results for the CSEE-FS-47 system.

Evaluation Indicator d_j	Weight W	Proposed Method	MIGA	SFCL Only	Switching Only
d_1	0.45	1.0000	1.0000	1.0000	1.0000
d_2	0.20	0.6027	0.2000	0.6000	0.2000
d_3	0.20	0.9991	0.8000	1.0000	0.8000
d_4	0.15	0.8021	0.2576	0.7352	0.2576
Comprehensive Evaluation Priority	1	0.8907	0.6886	0.8803	0.6886

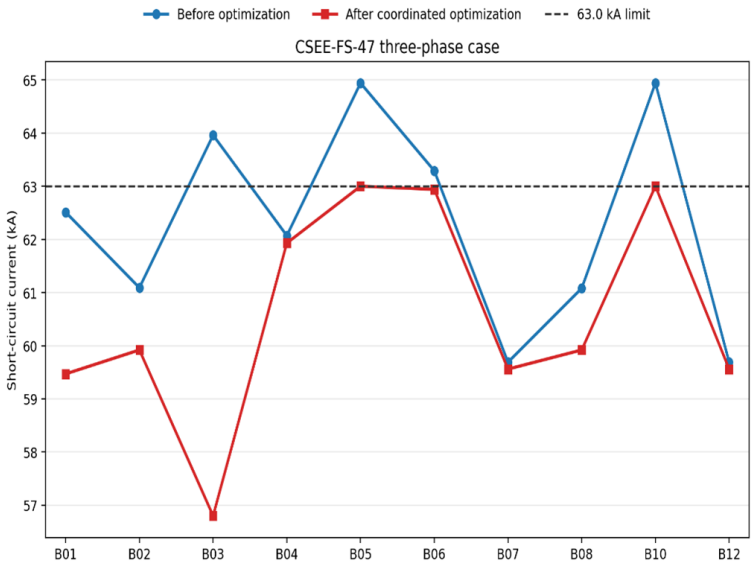


Figure 7. Short-circuit-current levels at the ten monitored buses before and after coordinated optimization in the CSEE-FS-47 system.

The comprehensive scores are 0.8907, 0.6886, 0.8803, and 0.6886 for the proposed, MIGA, SFCL-only, and switching-only plans. The proposed and SFCL-only methods perform closely. The baseline weights marginally favor the proposed method, whereas SFCL-only is 5.50% cheaper. The ranking is therefore interpreted under the stated baseline preferences rather than as a weight-independent result.

A selected single-component-outage short-circuit-current screening was conducted for the corrected coordinated scheme. The predefined screening set contains 10 line-outage cases associated with the monitored 525 kV network, 27 generator outages, and three HVDC bipole outages, for a total of 40 selected cases. The corresponding screening results are summarized in Table 13.

Table 13. Selected single-component-outage short-circuit-current screening results for the CSEE-FS-47 system; pass criterion: $I_{max} \leq 63.0$ kA.

Contingency Type	Selected Cases	Largest Current	Representative Worst Case	Cases with $I_{max} \leq 63.0$ kA
525 kV line outage	10	62.14 kA	B04-B06-1	10/10
Generator outage	27	62.11 kA	GEN-WT01-1	27/27
HVDC bipole outage	3	62.29 kA	DC01 bipole	3/3

All 40 selected outage cases satisfy the 63.0 kA short-circuit-current criterion. The category maxima are 62.14 kA for the 10 selected line outages, 62.11 kA for the 27 generator outages, and 62.29 kA for the three HVDC bipole outages. These results are limited to the predefined contingency set and the short-circuit-current criterion.

Overall, the corrected CSEE-FS-47 rerun demonstrates the applicability of the optimization workflow to a second benchmark but not the categorical dominance of one method. The proposed and SFCL-only methods achieve close comprehensive performance. The baseline weights slightly favor the proposed method (0.8907 versus 0.8803) because of its voltage-deviation and loss profile, whereas SFCL-only is 5.50% cheaper. On balance, the proposed method is mildly preferred when balanced operating performance is valued, while a cost-dominant decision maker may reasonably prefer SFCL-only.

6. Conclusions

To address the problem of excessive short-circuit currents in receiving-end power grids with multiple DC infeeds, this paper proposes a suppression strategy that integrates fuzzy comprehensive evaluation with coordinated optimization of grid structure and current-limiting devices.

The method was evaluated on the modified CSEE-VS-66 system under standard and high-load operating conditions, under a representative single-line-to-ground fault, and on the additional CSEE-FS-47 system. The conclusions are as followed:

1. The results confirm that relying exclusively on SFCL installation may require a relatively large total installed SFCL equivalent series resistance, whereas relying exclusively on topology adjustment may require more line disconnections. By coordinating targeted line openings with localized SFCL installation, the proposed method reduces the maximum three-phase short-circuit current from 65.16 to 62.96 kA under the standard operating condition and from 67.19 to 61.33 kA under the high-load operating condition. Its corresponding planning costs are 12.08% and 9.21% lower than those of the SFCL-only method and 48.67% and 29.98% lower than those of the switching-only method, respectively. Under the independently optimized single-line-to-ground case, the maximum current is reduced from 66.18 to 60.88 kA. The additional CSEE-FS-47 case demonstrates the applicability of the coordinated formulation to a different benchmark at the base operating point.
2. The proposed solution procedure adopts a sensitivity-assisted Benders-type architecture in which planning decisions are separated from simulation-based physical verification. The feedback coefficients are obtained from local finite-difference sensitivities and are interpreted as feasibility-guidance information rather than exact analytical

dual variables. In the investigated CSEE-VS-66 cases, the proposed method reaches a short-circuit-feasible solution after three iterations and requires substantially fewer BPA evaluations and shorter runtimes than MIGA. The additional CSEE-FS-47 case shows similar computational feasibility. Because the local guidance constraints approximate a nonconvex physical model, these results demonstrate practical convergence in the investigated cases but do not prove global convergence or global optimality.

3. The fuzzy comprehensive evaluation model provides a unified basis for comparing current-limiting achievement, steady-state voltage deviation, equipment investment, and network loss. Under the stated baseline weights, the proposed method scores 0.7557 in the standard CSEE-VS-66 case and 0.8180 in the high-load case. Switching-only ranks first in the standard case, while the proposed method ranks marginally first in the high-load case, although MIGA is 4.79% cheaper than the proposed scheme under the high-load condition. In the CSEE-FS-47 case, SFCL-only is 5.50% cheaper than the proposed method, whereas the proposed and SFCL-only methods obtain comprehensive scores of 0.8907 and 0.8803, respectively. These comparisons show that the methods can have close overall performance and that the final ranking is preference-dependent; the lowest investment cost or final short-circuit current does not necessarily identify the most balanced plan.
4. For the standard and high-load CSEE-VS-66 conditions, all configured line, generator, and HVDC contingencies satisfy the 63 kA short-circuit-current criterion after coordinated optimization. In CSEE-FS-47, the predefined set of 10 line, 27 generator, and three HVDC outage cases also satisfies this current criterion. These results document only selected-outage current screening and should not be interpreted as strict operational N-1 compliance, transient-voltage stability, frequency stability, or protection-coordination adequacy.

Future work will incorporate data-complete operational N-1 constraints, dynamic SFCL characteristics, transient AC/DC interactions, and protection-coordination requirements into the verification framework. These extensions will enable the planning results to be further assessed with respect to thermal loading, voltage recovery, relay operation, and equipment-level implementation requirements.

Author Contributions: Conceptualization, Y.C., X.Z. and Z.H.; methodology, Y.C., X.Z. and S.L.; software, X.L.; validation, S.L., P.G. and J.Z.; formal analysis, Y.C.; investigation, Y.C.; resources, J.Z. and Y.Z.; data curation, X.L.; writing—original draft preparation, Y.C.; writing—review and editing, Z.H. and Y.Z.; visualization, P.G.; supervision, Z.H.; project administration, Z.H. All authors have read and agreed to the published version of the manuscript.

Funding: This work was supported by the State Grid Corporation headquarters technology project of China (1400-202457360A-3-1-DG).

Data Availability Statement: The data and materials supporting the findings of this study are available from the corresponding author upon reasonable request. The available materials include the positive-sequence network input files, short-circuit calculation control cards, the single-line-to-ground fault control card, candidate branch lists, MATLAB R2026b source code, the fixed MIGA random seed (20260718, twister), and the saved numerical results used in the case studies. The commercial PSD-BPA software, executable files, and other licensed components are not included because they are subject to third-party licensing restrictions. Reproduction of the PSD-BPA-based calculations therefore requires authorized access to a compatible version of the software. The single-line-to-ground fault control card available upon request contains the conversion settings used in the reported calculation; no separate zero-sequence network-data file was used or generated.

Conflicts of Interest: Authors Yang Cao, Shanhe Liu, Xiaofei Li, Pan Gu, Jingyi Zhang and Yan Zhang were employed by the company State Grid Economic and Technological Research Institute Co., Ltd., Beijing, China. Author Xudong Zhang was employed by the company State Grid Corporation of China (China), Beijing, China. The remaining authors declare that the research was conducted in the absence of any commercial or financial relationships that could be construed as a potential conflict of interest. The authors declare that this study received funding from the State Grid Corporation headquarters technology project of China (1400-202457360A-3-1-DG). The funder was not involved in the study design, collection, analysis, interpretation of data, the writing of this article or the decision to submit it for publication.

Abbreviations

The following abbreviations are used in this manuscript:

DC	Direct Current
AC	Alternating Current
UHVDC	Ultra-High-Voltage Direct Current
LCC-HVDC	Line Commutated Converter-Based High Voltage Direct Current
SFCL	Superconducting Fault Current Limiter
RMS	Root Mean Square
MINLP	Mixed-Integer Nonlinear Programming
MILP	Mixed-Integer Linear Programming
MP	Master Problem
SP	Subproblem
AHP	Analytic Hierarchy Process

Appendix A. System Parameters

Appendix A.1. Modified CSEE-VS-66 System

Table A1. 525-kV AC-Line Parameters.

NO.	From Bus	To Bus	Voltage (kV)	R (p.u.)	X (p.u.)	B (p.u.)	Circuit
1	B02	B01	525	0.00040	0.00910	0.00615	1
2	B03	B02	525	0.00010	0.00400	0.00210	1
3	B04	B01	525	0.00040	0.00420	0.00327	1
4	B04	B02	525	0.00040	0.00420	0.00578	1
5	B04	B03	525	0.00009	0.00010	0.00129	1
6	B04	B07	525	0.00020	0.00500	0.00400	1
7	B05	B03	525	0.00080	0.00800	0.00450	2
8	B05	B08	525	0.00080	0.00800	0.00140	1
9	B06	B05	525	0.00020	0.00200	0.00210	1
10	B07	B10	525	0.00008	0.00085	0.00321	1
11	B08	B06	525	0.00020	0.00270	0.00190	1
12	B08	B09	525	0.00010	0.00270	0.00170	1
13	B08	B11	525	0.00040	0.00760	0.00450	1
14	B09	B06	525	0.00040	0.00610	0.00840	1
15	B12	B10	525	0.00090	0.00110	0.00157	1
16	B12	B11	525	0.00050	0.00630	0.00351	1
17	B13	B05	525	-	0.00010	-	1
18	B14	B06	525	0.00009	0.00098	0.00306	1
19	B15	B07	525	0.00007	0.00080	0.00251	1
20	B16	B09	525	0.00009	0.00098	0.00306	1
21	B17	B12	525	0.00006	0.00012	0.00010	1
22	B18	B06	525	0.00030	0.00380	0.01840	1
23	B19	B11	525	0.00070	0.00980	0.01840	1
24	B67	B02	525	-	0.00010	-	1

Table A2. Two-Winding Transformer Parameters.

No.	From Bus	To Bus	Rated Capacity (MVA)	Leakage Reactance (p.u.)	Tap Voltage (kV)	Parallel Units
1	B21	DP-01	3000	0.00600	525/210.4	1
2	B13	DP-02	3000	0.00600	525/199.4	1
3	B21	DN-01	3000	0.00600	525/210.4	1
4	B13	DN-02	3000	0.00600	525/199.4	1
5	B68	DP-03	3000	0.00600	525/210.4	1
6	B67	DP-04	3000	0.00600	525/199.4	1
7	B68	DN-03	3000	0.00600	525/210.4	1
8	B67	DN-04	3000	0.00600	525/199.4	1
9	COND1	B05	8000	0.00350	20/525	1
10	WT19-01	B32	450	0.01389	0.69/38.5	1
11	WT19-02	B32	450	0.01389	0.69/38.5	1
12	WT19-03	B32	450	0.01389	0.69/38.5	1
13	B24	B32	300	0.03500	230/38.5	4
14	WT01-01	B33	450	0.01389	0.69/38.5	1
15	WT01-02	B33	450	0.01389	0.69/38.5	1
16	WT01-03	B33	450	0.01389	0.69/38.5	1
17	B26	B33	300	0.03500	230/38.5	4
18	PV18-01	B31	300	0.02167	0.40/38.5	2
19	PV18-02	B31	300	0.02167	0.40/38.5	2
20	PV18-03	B31	300	0.02167	0.40/38.5	2
21	B22	B31	300	0.03500	230/38.5	4
22	TP14-01	B14	750	0.02671	20/525	1
23	TP15-01	B15	750	0.02671	20/525	1
24	TP16-01	B16	750	0.03331	20/525	1
25	TP17-01	B17	750	0.03331	20/525	1

Table A3. Three-Winding Transformer Parameters.

No.	Transformer	Connected Buses	X_1 (p.u.)	X_2 (p.u.)	X_3 (p.u.)	Rated Capacity (MVA)
1	T3-01	B18/B23/B28	0.01637	−0.00190	0.01922	1500/1500/450
2	T3-02	B19/B25/B29	0.01637	−0.00190	0.01922	1500/1500/450
3	T3-03	B01/B27/B30	0.01637	0.00190	0.01922	1500/1500/450
4	T3-04	B01/B34/B35	0.01570	−0.00158	0.02668	1000/1000/360
5	T3-05	B02/B36/B37	0.01570	−0.00158	0.02668	1000/1000/360
6	T3-06	B03/B38/B39	0.01570	−0.00158	0.02668	1000/1000/360
7	T3-07	B04/B40/B41	0.01570	−0.00158	0.02668	1000/1000/360
8	T3-08	B05/B42/B43	0.01570	−0.00158	0.02668	1000/1000/360
9	T3-09	B06/B44/B45	0.01570	−0.00158	0.02668	1000/1000/360
10	T3-10	B07/B46/B47	0.01570	−0.00158	0.02668	1000/1000/360
11	T3-11	B08/B48/B49	0.01570	−0.00158	0.02668	1000/1000/360
12	T3-12	B09/B50/B51	0.01570	−0.00158	0.02668	1000/1000/360
13	T3-13	B10/B52/B53	0.01570	−0.00158	0.02668	1000/1000/360
14	T3-14	B11/B54/B55	0.01570	−0.00158	0.02668	1000/1000/360
15	T3-15	B12/B56/B57	0.01570	−0.00158	0.02668	1000/1000/360

Table A4. Synchronous Generator Parameters under Normal- and High-Load Conditions.

No.	Generator	Bus Type	P_{max} (MW)	Q_{max} (Mvar)	V_{set} (p.u.)	P_G^N (MW)	P_G^H (MW)
1	TP14-01	Slack	900	3000	1.05	283.4	681.7
2	TP15-01	PV	900	800	1.00	800.0	864.6
3	TP16-01	PV	900	800	1.00	800.0	864.6
4	TP17-01	PV	900	800	1.00	800.0	864.6

Table A5. Renewable Energy Parameters.

No.	Main-Grid Bus	Renewable Unit	Type	Rated Capacity (MW)
1	B01	WT01-01	Wind	400
2	B01	WT01-02	Wind	400
3	B01	WT01-03	Wind	400
4	B18	PV18-01	PV	400
5	B18	PV18-02	PV	400
6	B18	PV18-03	PV	400
7	B19	WT19-01	Wind	400
8	B19	WT19-02	Wind	400
9	B19	WT19-03	Wind	400

Table A6. Load and Static Reactive Compensation Capacities under Normal- and High-Load Conditions.

Main-Grid Bus	P_L^N (MW)	Q_L^N (Mvar)	P_L^H (MW)	Q_L^H (Mvar)	Compensation (Mvar)
B01	284.8	98.4	327.5	113.2	160
B02	326.4	119.2	375.4	137.1	160
B03	271.2	97.6	311.9	112.2	160
B04	361.6	132.0	415.8	151.8	160
B05	404.8	129.6	465.5	149.0	160
B06	380.0	123.2	437.0	141.7	150
B07	365.6	125.6	420.4	144.4	180
B08	376.0	128.0	432.4	147.2	180
B09	319.2	92.0	367.1	105.8	150
B10	407.2	132.8	468.3	152.7	180
B11	341.6	113.6	392.8	130.6	160
B12	85.6	25.6	98.4	29.4	60
Total	**3924.0**	**1317.6**	**4512.6**	**1515.2**	**1860**

Appendix A.2. Modified CSEE-FS-47 System

Table A7. 525-kV AC-Line Parameters of the CSEE-FS-47 System.

No.	From Bus	To Bus	R (p.u.)	X (p.u.)	B (p.u.)	Voltage (kV)	Circuits
1	B01	B02	0.00005	0.00168	0.03788	525	1
2	B01	B03	0.00025	0.00158	0.19970	525	1
3	B01	B04	0.00070	0.00920	0.10159	525	1
4	B02	B04	0.00057	0.00799	0.44622	525	1
5	B04	B06	0.00011	0.00153	0.00287	525	2
6	B03	B05	0.00007	0.00095	0.00179	525	1
7	B05	B06	0.00005	0.00166	0.00125	525	1
8	B06	B07	0.00040	0.00550	0.01020	525	2
9	B02	B07	0.00025	0.00358	0.19970	525	1

Table A8. Two-Winding Transformer Parameters of the CSEE-FS-47 System.

No.	Transformer	X (p.u.)	Rated Capacity (MVA)	Rated Voltage (kV)	Turns Ratio	Units
1	T2-01/T2-02/T2-04/T2-07	0.01064	780	20/525	1.000	4
2	T2-03/T2-05/T2-06	0.01064	1400	20/525	1.000	3
3	T2-08–T2-16	0.01806	350	0.69/38.5	1.000	9
4	T2-17–T2-27	0.02167	350	0.40/38.5	1.000	11
5	T2-28–T2-47	0.03500	350	38.5/230	1.000	20

Table A9. Three-Winding Transformer Parameters of the CSEE-FS-47 System.

No.	Transformer	X_1 (p.u.)	X_2 (p.u.)	X_3 (p.u.)	Rated Capacity (MVA)	Units
1	T3-01–T3-09	0.01570	−0.00158	0.02668	1000/1000/360	9
2	T3-10–T3-15	0.02143	−0.00210	0.04093	1000/1000/300	6

Table A10. Synchronous-Generator Parameters of the CSEE-FS-47 System.

No.	Generator	Bus Type	Rated Capacity (MVA)	Rated Active Power (MW)
1	HP01	PV	667	600
2	HP02	Slack	667	600
3	HP03	PV	1150	1000
4	HP04	PV	667	600
5	HP05	PV	1150	1000
6	HP06	PV	1150	1000
7	HP07	PV	667	600

Table A11. Renewable-Energy Unit Parameters of the CSEE-FS-47 System.

No.	Unit	Type	Bus Type	Rated Capacity (MVA)
1	WT01-1	Wind power	PQ	350
2	WT01-2	Wind power	PQ	350
3	WT01-3	Wind power	PQ	350
4	WT03-1	Wind power	PQ	350
5	WT03-2	Wind power	PQ	350
6	WT03-3	Wind power	PQ	350
7	WT05-1	Wind power	PQ	350
8	WT05-2	Wind power	PQ	350
9	WT05-3	Wind power	PQ	350
10	PV01-1	Photovoltaic	PQ	350
11	PV01-2	Photovoltaic	PQ	350
12	PV01-3	Photovoltaic	PQ	350
13	PV03-1	Photovoltaic	PQ	350
14	PV03-2	Photovoltaic	PQ	350
15	PV03-3	Photovoltaic	PQ	350
16	PV03-4	Photovoltaic	PQ	300
17	PV03-5	Photovoltaic	PQ	300
18	PV05-1	Photovoltaic	PQ	350
19	PV05-2	Photovoltaic	PQ	350
20	PV05-3	Photovoltaic	PQ	350

Table A12. Load and Static Reactive-Power Compensation Data of the CSEE-FS-47 System.

Associated 525-kV Bus	Load Bus	P_L (MW)	Q_L (Mvar)	Static Compensation Buses	Q_C (Mvar)
B01	B56	360.0	168.0	B14/B49/B62	130
B02	B57	360.0	120.0	B63	40
B03	B58	360.0	132.0	B15/B50/B51/B64	160
B04	B59	394.8	213.6	B65	40
B05	B60	360.0	84.0	B16/B54/B66	100
B07	B61	387.6	94.8	B67	40
Total	–	**2222.4**	**812.4**	–	**510**

References

1. Deng, B.; Wen, Y. Coordinated expansion planning of AC network and synchronous condenser for receiving-end grids with multi-infeed UHVDC links. *CSEE J. Power Energy Syst.* **2024**, *12*, 2380–2393. [CrossRef]
2. Zhang, F.; Xin, H.; Wu, D.; Wang, Z.; Gan, D. Assessing strength of multi-infeed LCC-HVDC systems using generalized short-circuit ratio. *IEEE Trans. Power Syst.* **2019**, *34*, 467–480. [CrossRef]
3. Xiao, H.; Zhang, Y.; Duan, X.; Li, Y. Evaluating strength of hybrid multi-infeed HVDC systems for planning studies using hybrid multi-infeed interactive effective short-circuit ratio. *IEEE Trans. Power Deliv.* **2021**, *36*, 2129–2142. [CrossRef]
4. Fan, X.; Zhang, Y.; Su, L.; Liu, H.; Cui, R.; Wei, Y. Research on short circuit current control in multi-infeed DC receiving power grid. *Smart Power* **2018**, *46*, 61–67.
5. Lin, J. Research on Short-Circuit Current Limitation Measures for the North Hebei Power Grid. Ph.D. Thesis, North China Electric Power University, Baoding, China, 2014.
6. Li, S.; Ren, Y.; Gu, X.; Cao, X.; Yang, X. Optimization of transmission network structure based on explicit linear modeling of short circuit current constraints. *Trans. China Electrotech. Soc.* **2020**, *35*, 3292–3302.
7. Tian, S.; Wang, X.; Wang, X.; Qi, S.; Dou, X. Short-circuit current limitation method of large scale power system based on network reconfiguration. *Smart Power* **2018**, *46*, 6–12.
8. Han, B.; Chen, W.; Chang, N.; Jin, Y.; Qie, X.; Han, Y.; Zhu, B.; Tan, S.; Yu, Y.; Zhang, J.; et al. Short-circuit Current Limitation Based on Dynamic Adjustment of System Topology. *Power Syst. Technol.* **2021**, *45*, 1158–1166.
9. Lee, G.S.; Kwon, D.H.; Moon, S.I.; Kim, C.K.; Lee, J.; Kim, J. A coordinated control strategy for LCC HVDC systems for frequency support with suppression of AC voltage fluctuations. *IEEE Trans. Power Syst.* **2020**, *35*, 2804–2814. [CrossRef]
10. Abramovitz, A.; Smedley, K.M. Survey of solid-state fault current limiters. *IEEE Trans. Power Electron.* **2012**, *27*, 2770–2782. [CrossRef]
11. Lu, W.; Liu, Y.; Zhou, Q.; Fang, T.; Wang, Z.; Zhang, G. Fast-swiching high voltage fault current limiter with multiple breakers. *Autom. Electr. Power Syst.* **2019**, *43*, 234–241.
12. Zheng, J. Current status and application prospect of fault current limiters. *Proc. CSEE* **2014**, *34*, 5140–5148.
13. Huo, R.; Huang, W.; Yu, M.; Tai, N.; Yao, G.; Wang, Y. Protection method for transient high-frequency voltage-to ground in ring DC microgrid with current limiting reactor. *Autom. Electr. Power Syst.* **2023**, *47*, 127–136.
14. Hu, W.; Wei, Z.; Sun, G.; Li, Q.; Liu, J. Optimal allocation of superconducting fault current limiters based on sensitivity method. *Autom. Electr. Power Syst.* **2012**, *36*, 62–67.
15. Ye, C.; Huang, M.; Chen, L.; Liu, C. Multi objective current limiters configuration based on parallel fast and elitist non-dominated sorting genetic algorithm-2. *Autom. Electr. Power Syst.* **2013**, *37*, 49–55.
16. Zhu, S.; Zhao, C.; Li, C.; Xu, J. Optimal configuration of current-limiting reactor considering fault current limiter action in DC grid. *Autom. Electr. Power Syst.* **2018**, *42*, 142–149.
17. Li, C.; Wu, Y.; Sun, Y.; Zhang, H.; Liu, Y.; Liu, Y.; Terzija, V. Continuous under-frequency load shedding scheme for power system adaptive frequency control. *IEEE Trans. Power Syst.* **2020**, *35*, 950–959. [CrossRef]
18. Bynum, M.; Castillo, A.; Watson, J.-P.; Laird, C.D. Tightening McCormick relaxations toward global solution of the ACOPF problem. *IEEE Trans. Power Syst.* **2019**, *34*, 814–824. [CrossRef]
19. Deng, B.; Wen, Y.; Yu, L.; Jiang, X. Short-circuit Current Suppression Strategy for Receiving-end Power Grid Based on Coordination of Current Limiter Configuration and Network Structure Optimization. *Autom. Electr. Power Syst.* **2024**, *48*, 152–161.
20. Zhang, Y.; Cai, Z.; Li, A.; Xu, M. An optimization algorithm for short-circuit current limitation of 500 kV power grid by adjusting power grid configuration. *Autom. Electr. Power Syst.* **2009**, *33*, 34–39.
21. Li, S.; Zhang, Y.; Gu, X.; Yan, L. Optimal transmission switching strategy for multi-infeed DC receiving-end power network to prevent over-limit of short-circuit current. *IET Gener. Transm. Distrib.* **2023**, *17*, 5062–5073. [CrossRef]
22. Wu, C.; Liu, M.; Zhang, Z.; Xie, M. A heuristic decomposition algorithm to optimally configure superconducting fault current limiters in large-scale power systems. *Int. J. Electr. Power Energy Syst.* **2025**, *167*, 110606. [CrossRef]
23. Füllner, C.; Rebennack, S. Non-convex nested Benders decomposition. *Math. Program.* **2022**, *196*, 987–1024. [CrossRef]
24. Zhao, B.; Xu, S.; Lan, T.; Sun, H. Benchmark for AC-DC Hybrid System with High Penetration of Renewables (III): Voltage Stability Benchmark CSEE-VS. *Proc. CSEE* **2024**, *44*, 8353–8364.
25. Wu, P.; Zhao, B.; Cheng, Y.; Sun, H. Benchmark for AC–DC Hybrid System with High Penetration of Renewables (II): Frequency Stability CSEE-FS. *Proc. CSEE* **2024**, *44*, 7531–7542.

Disclaimer/Publisher's Note: The statements, opinions and data contained in all publications are solely those of the individual author(s) and contributor(s) and not of MDPI and/or the editor(s). MDPI and/or the editor(s) disclaim responsibility for any injury to people or property resulting from any ideas, methods, instructions or products referred to in the content.